Lactate is an energy substrate for rodent cortical neurons and enhances their firing activity

Anastassios Karagiannis, Thierry Gallopin, Alexandre Lacroix, Fabrice Plaisier, Juliette Piquet, Hélène Geoffroy, Régine Hepp, Jérémie Naudé, Benjamin Le Gac, Richard Egger, et al.

Lactate is an energy substrate for rodent cortical neurons and enhances their firing activity.

Anastassios Karagiannis[1], Thierry Gallopin[2], Alexandre Lacroix[1], Fabrice Plaisier[1], Juliette Piquet[1], Hélène Geoffroy[2], Régine Hepp[1], Jérémie Naudé[1], Benjamin Le Gac[1], Richard Egger[3], Bertrand Lambolez[1], Dongdong Li[1], Jean Rossier[1,2], Jochen F. Staiger[4], Hiromi Imamura[5], Susumu Seino[6], Jochen Roeper[3] and Bruno Cauli[1*].

1. Sorbonne Université, CNRS, INSERM, Neurosciences Paris Seine - Institut de Biologie Paris Seine (NPS-IBPS), 9 quai Saint Bernard, 75005 Paris, France.

2. Brain Plasticity Unit, CNRS, ESPCI Paris, PSL Research University, 10 rue Vauquelin, 75005 Paris, France.

3. Institute of Neurophysiology, Goethe University Frankfurt, Theodor-Stern-Kai 7, 60590 Frankfurt, Germany.

4. Institute for Neuroanatomy, University Medical Center Göttingen, Georg-August-University Göttingen, 37075 Göttingen, Germany.

5. Graduate School of Biostudies, Kyoto University, Kyoto 606-8501, Japan.

6. Division of Molecular and Metabolic Medicine, Kobe University Graduate School of Medicine, 7-5-1 Kusunoki-cho, Chuo-ku, Kobe, Hyogo 650-0017, Japan.

*Correspondence: bruno.cauli@upmc.fr

Summary

Glucose is the mandatory fuel for the brain, yet the relative contribution of glucose and lactate for neuronal energy metabolism is unclear. We found that increased lactate, but not glucose concentration, enhances the spiking activity of neurons of the cerebral cortex. Enhanced spiking was dependent on ATP-sensitive potassium (K_{ATP}) channels formed with KCNJ11 and ABCC8 subunits, which we show are functionally expressed in most neocortical neuronal types. We also demonstrate the ability of cortical neurons to take-up and metabolize lactate. We further reveal that ATP is produced by cortical neurons largely via oxidative phosphorylation and only modestly by glycolysis. Our data demonstrate that in active neurons, lactate is preferred to glucose as an energy substrate, and that lactate metabolism shapes neuronal activity in the neocortex through K_{ATP} channels. Our results highlight the importance of metabolic crosstalk between neurons and astrocytes for brain function.

Impact Statement

Lactate is preferred to glucose as an energy substrate and exacerbates spiking activity in most neuron types of juvenile somatosensory cortex by closing ATP-sensitive potassium channels.

Keywords

K_{ATP} channel, pyramidal cell, interneuron, glucose, single cell RT-PCR, ATP.

Highlights

- Most cortical neuron subtypes express functional K_{ATP} channels.
- Lactate enhances spiking activity via its uptake and closure of K_{ATP} channels.
- Cortical neurons take up and oxidize lactate.
- Cortical neurons produce ATP mainly by oxidative phosphorylation.

Introduction

The human brain represents 2% of the body mass, yet it consumes about 20% of blood oxygen and glucose which are mandatory energy substrates (Clarke and Sokoloff, 1999). The majority (~50-80%) of the cerebral energy metabolism is believed to be consumed by the Na^+/K^+ ATPase pump to maintain cellular ionic gradients dissipated during synaptic transmission and action potentials (Attwell and Laughlin, 2001;Lennie, 2003). Synaptic and spiking activities are also coupled with local cerebral blood flow and glucose uptake (Devor et al., 2008;Logothetis, 2008). This process, referred to as neurovascular and neurometabolic coupling, is the physiological basis of brain imaging techniques (Raichle and Mintun, 2006) and maintains extracellular glucose within a physiological range of 2-3 mM (Silver and Erecinska, 1994;Hu and Wilson, 1997b). Also, following increased neuronal activity extracellular lactate increases (Prichard et al., 1991;Hu and Wilson, 1997a) for several minutes up to twice of its 2-5 mM basal concentration despite oxygen availability (Magistretti and Allaman, 2018).

Based on the observations that various by-products released during glutamatergic transmission stimulate astrocyte glucose uptake, aerobic glycolysis and lactate release (Pellerin and Magistretti, 1994;Voutsinos-Porche et al., 2003;Ruminot et al., 2011;Choi et al., 2012;Sotelo-Hitschfeld et al., 2015;Lerchundi et al., 2015), lactate has been proposed to be shuttled from astrocytes to neurons to meet neuronal energy needs. This hypothesis is supported by the existence of a lactate gradient between astrocytes and neurons (Machler et al., 2016), the preferential use of lactate as an energy substrate in cultured neurons (Bouzier-Sore et al., 2003;Bouzier-Sore et al., 2006), and its ability to support neuronal activity during glucose shortage (Schurr et al., 1988;Rouach et al., 2008;Wyss et al., 2011;Choi et al., 2012). However, the use of different fluorescent glucose analogues to determine whether astrocytes or neurons take up more glucose during sensory-evoked neuronal activity has led to contradicting results (Chuquet et al., 2010;Lundgaard et al., 2015). Furthermore brain slices and *in vivo* evidence have indicated that synaptic and sensory stimulation enhanced neuronal glycolysis and potentially lactate release by neurons (Ivanov et al., 2014;Diaz-Garcia et al., 2017), thereby challenging the astrocyte-neuron lactate shuttle hypothesis. Hence, the relative contribution of glucose and lactate to neuronal ATP synthesis remains unresolved.

ATP-sensitive potassium channels (K_{ATP}) act as metabolic sensors controlling various cellular functions (Babenko et al., 1998). Their open probability (P_o) is regulated by the energy charge of the cell (*i.e.* the ATP/ADP ratio). While ATP mediates a tonic background inhibition of K_{ATP} channels, cytosolic increases of ADP concentrations that occur as a sequel to enhanced energy demands, increase the P_o of K_{ATP} channels. In neurons, electrical activity is accompanied by enhanced sodium influx, which in turn activates the Na^+/K^+ ATPase. Activity of this pump alters the submembrane ATP/ADP ratio sufficiently to activate K_{ATP} channels (Tanner et al., 2011). The use of fluorescent ATP/ADP biosensors has demonstrated that K_{ATP} channels are activated (P_o>0.1) when ATP/ADP ratio is ≤ 5 (Tantama et al., 2013).

K_{ATP} channels are heterooctamers composed of four inwardly rectifying K^+ channel subunits, KCNJ8 (previously known as Kir6.1) or KCNJ11 (previously known as Kir6.2), and four sulfonylurea receptors, ABCC8 (previously known as SUR1) or ABCC9 (previously known as SUR2), the later existing in two splice variants (SUR2A and SUR2B) (Sakura et al., 1995;Aguilar-Bryan et al., 1995;Inagaki et al., 1995b;Isomoto et al., 1996;Inagaki et al., 1996;Chutkow et al., 1996;Yamada et al., 1997;Li et al., 2017;Martin et al., 2017;Lee et al., 2017;Puljung, 2018). The composition in K_{ATP} channel subunits confers different functional properties, pharmacological profiles as well as metabolic sensitivities (Isomoto et al., 1996;Inagaki et al., 1996;Gribble et al., 1997;Yamada et al., 1997;Okuyama et al., 1998;Liss et al., 1999). K_{ATP} channel subunits are expressed in the neocortex (Ashford et al., 1988;Karschin et al., 1997;Dunn-Meynell et al., 1998;Thomzig et al., 2005;Cahoy et al., 2008;Zeisel et al., 2015;Tasic et al., 2016) and have been shown to protect cortical neurons from ischemic injury (Heron-Milhavet et al., 2004;Sun et al., 2006) and to modulate their excitability (Gimenez-Cassina et al., 2012) and intrinsic firing activity (Lemak et al., 2014). K_{ATP} channels could thus be leveraged to decipher electrophysiologically the relative contribution of glucose and lactate to neuronal ATP synthesis. Here, we apply single-cell RT-PCR (scRT-PCR) to identify the mRNA subunit composition of K_{ATP} channel across different neocortical neuron subtypes and demonstrate lactate as the preferred energy substrate that also enhances firing activity.

Results

Expression of K_{ATP} channel subunits in identified cortical neurons

We first sought to determine whether K_{ATP} channel subunits were expressed in different neuronal subtypes from the neocortex. Neurons (n=277) of the juvenile rat barrel cortex from layers I to IV (Supplementary file 1) were functionally and molecularly characterized in acute slices by scRT-PCR (Figure 1), whose sensitivity was validated from 500 pg of total cortical RNAs (Figure 1-figure supplement 1A). Neurons were segregated into 7 different subtypes according to their overall molecular and electrophysiological similarity (Figure 1A) using unsupervised Ward's clustering (Ward, 1963), an approach we previously successfully used to classify cortical neurons (Cauli et al., 2000;Gallopin et al., 2006;Karagiannis et al., 2009). Regular spiking (RS, n=63) and intrinsically bursting (IB, n=10) cells exhibited the molecular characteristics of glutamatergic neurons, with very high single-cell detection rate (n=69 of 73, 95%) of vesicular glutamate transporter 1 (*Slc17a7*) and low detection rate (n=7 of 73, 10%) of glutamic acid decarboxylases (*Gad*s, Figure 1B-E and Supplementary file 2), the GABA synthesizing enzymes. This group of glutamatergic neurons distinctly displayed hyperpolarized resting membrane potential (-81.2 ± 0.8 mV), possessed a large membrane capacitance (108.6 ± 3.6 pF), discharged with wide action potentials (1.4 ± 0.0 ms) followed by medium afterhyperpolarizations (mAHs). These neurons did sustain only low maximal frequencies (35.4 ± 1.6 Hz) and showed complex spike amplitude accommodation (Supplementary file 5). In contrast to RS neurons, IB neurons were more prominent in deeper layers (Supplementary file 1) and their bursting activity affected their adaptation amplitudes and kinetics (Figure 1C and Supplementary files 4,5), spike broadening (Figure 1C and Supplementary file 6) and the shape of mAHs (Figure 1C and Supplementary file 7).

All other neuronal subtypes were characterized by a high single-cell detection rate of *Gad2* and/or *Gad1* mRNA (n=202 of 204, 99%, Figure 1B and Supplementary file 2) and therefore likely corresponded to GABAergic interneurons. Among *Gad*-positive population, neurons were frequently positive for vasoactive intestinal polypeptide (*Vip*) mRNA, and in accordance to their electrophysiological phenotypes, were segregated into Bursting *Vip* (n=27) and Adapting *Vip* (n=59) neurons. These *Vip* interneurons were further characterized by high membrane resistance (581 ± 27 MΩ)

and small membrane capacitance (52.7 ± 2.3 pF, Figure 1B-C and Supplementary file 3).

In other GABAergic interneurons somatostatin (*Sst*) and calbindin (*Calb1*) as well as neuropeptide Y (*Npy*) to a lesser extent, were frequently detected and functionally corresponded to Adapting *Sst* neurons (n=24, Figure 1B and Supplementary file 2). They displayed depolarized resting membrane potential, pronounced voltage sags, low rheobases and pronounced afterdepolarizations (Figure 1C and Supplementary files 3-4,7). In another group of GABAergic adapting interneurons located in superficial layers, mRNA for *Npy* was detected at a high rate (n=31 of 56, 55%). In these Adapting NPY interneurons mRNA for nitric oxide synthase-1 (*Nos1*) was detected at a lower rate (Figure 1B and Supplementary files 1,2). In response to suprathreshold depolarizing current steps, these interneurons showed very little spike frequency adaptation (Figure 1C and Supplementary file 4). Finally, parvalbumin (*Pvalb*) was observed in virtually all neurons of a subpopulation termed Fast Spiking-*Pvalb* interneurons (FS-*Pvalb*, n=37 of 38, 97%, Figure 1B and Supplementary file 2). In comparison to all other cortical neurons described above, they were characterized by low membrane resistance (201 ± 13 MΩ), fast time constant, high rheobase, very short spikes (0.6 ± 0.0 ms) with sharp fast afterhyperpolarizations (fAHs) and the ability to sustain high firing rates (139.9 ± 6.8 Hz) with little to no frequency adaptation (Figure 1C and Supplementary files 3-7). These data thus identified different neuronal subtypes based on their distinctive electrophysiological and molecular features (Ascoli et al., 2008) confirming our previous classification schemes (Cauli et al., 2000;Gallopin et al., 2006;Karagiannis et al., 2009).

The functional and molecular classification of cortical neurons allowed us to probe for the single-cell expression of mRNA for K_{ATP} channel subunits (Figure 1-figure supplement 1A) in well defined subpopulations. Apart from a single Adapting *Npy* neuron (Figure 1D), where *Kcnj8* mRNA was observed, only the *Kcnj11* and *Abcc8* subunits were detected in cortical neurons (in 25%, n=63 of 248 neurons; and in 10%, n=28 of 277 of neurons; respectively). The single-cell detection rate was similar between the different neuronal subtypes (Figure 1F). We also codetected *Kcnj11* and *Abcc8* in cortical neurons (n=14 of 248, Figure 1D) suggesting the expression of functional K_{ATP} channels.

Characterization of K_{ATP} channels in cortical neurons

To assess functional expression of K_{ATP} channels in identified cortical neurons (n=18, Figure 2A), we measured the effects of different K_{ATP} channel modulators on whole-cell currents ($Q_{(3,18)}$=32.665, p=3.8 x 10^{-7}, Friedman test) and membrane resistances ($Q_{(3,18)}$=40.933, p=6.8 x 10^{-9}). Pinacidil (100 µM), an ABCC9-preferring K_{ATP} channel opener (Inagaki et al., 1996;Moreau et al., 2005), had little or no effect on current (4.1 ± 3.7 pA, p=0.478) and membrane resistance (-9.6 ± 3.7 %, p=0.121, Figure 2B-C). By contrast, diazoxide (300 µM), an opener acting on ABCC8 and SUR2B-containing K_{ATP} channels (Inagaki et al., 1996;Moreau et al., 2005), consistently induced an outward current (45.0 ± 9.6 pA, p=4.8 x 10^{-5}) and a decrease in membrane resistance (-34.5 ± 4.3%, p=3.6 x 10^{-5}) indicative of the activation of a hyperpolarizing conductance (Figure 2B-C). The sulfonylurea tolbutamide (500 µM, Figure 2B-C), a K_{ATP} channel blocker (Ammala et al., 1996;Isomoto et al., 1996;Gribble et al., 1997;Isomoto and Kurachi, 1997), did not change whole-cell basal current (-6.6 ± 3.0 pA, p=0.156) or membrane resistance (20.5 ± 7.5%, p=3.89 x 10^{-2}). Conversely, tolbutamide dramatically reversed diazoxide effects on both current (p=4.1 x 10^{-8}) and membrane resistance (p=5.8 x 10^{-10}).

All pharmacologically analyzed neurons (n=63) exhibited a more positive whole-cell current (ΔI=53 ± 6 pA, range: 4 to 228 pA) and a lower membrane resistance (ΔR_m=-270 ± 31 MΩ, range: -17 to -1221 MΩ) under diazoxide than under tolbutamide, indicative of their sensitivy to K_{ATP} channel manipulation. In virtually all neuronal subtypes ($H_{(6,43)}$=2.274, p=0.810, Kruskal–Wallis H test) or groups ($t_{(42)}$=0.3395, p=0.736, Student's t-test), the diazoxide-tolbutamide current/voltage relationship reversed very close to the theoretical potassium equilibrium potential (E_K=-106.0 mV, Figure 2D-F) confirming the opening of a selective potassium conductance. Besides its effects on plasma membrane K_{ATP} channels, diazoxide is also a mitochondrial uncoupler (Drose et al., 2006) which increases reactive oxygen species (ROS) production. This might stimulate Ca^{2+} sparks and large-conductance Ca^{2+}-activated potassium channels (Xi et al., 2005) leading to potential confounding effects. This possibility was ruled out by the observation that Mn(III)tetrakis(1-methyl-4-pyridyl)porphyrin (MnTMPyP, 25 µM), a ROS scavenger (D'Agostino et al., 2007), did not reduce the diazoxide-tolbutamide responses on current ($t_{(10)}$=0.76559, p=0.462, Figure 2-figure supplement 1A,B) and conductance ($t_{(10)}$=1.24758, p=0.241, Figure 2-figure supplement 1A,C).

Cortical neurons exhibited K_{ATP} conductances of similar value between their subtypes ($H_{(6,63)}$=5.6141, p=0.468) or groups ($U_{(9,54)}$=233, p=0.855, Mann–Whitney U test, Figures S3A,B). K_{ATP} channels activated by diazoxide essentially doubled the whole cell conductance in the subthreshold membrane potential compared to control or tolbutamide conditions, regardless of neuronal subtypes ($H_{(6,63)}$=5.4763, p=0.484) or groups ($t_{(61)}$=1.324, p=0.191, Figures 2G,H). Also, K_{ATP} current density was similar ($H_{(6,63)}$=4.4769, p=0.612, $U_{(9,54)}$=240.5, p=0.965, Figure 2-figure supplement 2C,D). Twenty nine diazoxide/tolbutamide-responsive neurons were successfully characterized by scRT-PCR. *Kcnj11* and *Abcc8* mRNAs were detected in 35% (n=10 of 29) and 7% (n=2 of 29) of these neurons, respectively. These proportions are low compared to the pharmacological responsiveness but similar to the whole sample of profiled cortical neurons (p=0.3721 and p=1.0000, Fisher's exact test). These observations suggest that *Kcnj11* and *Abcc8* subunits were underdetected by scRT-PCR mRNA profiling. Together with the pinacidil unresponsiveness and the lack of *Abcc9* detection, these data indicate that the large majority of cortical neurons express functional ABCC8-mediated K_{ATP} channels across different subpopulations. To confirm that KCNJ11 is the pore-forming subunit of K_{ATP} channels in cortical neurons, we used a genetic approach based on *Kcnj11* knock-out mice (Miki et al., 1998). We first verified that *Kcnj11* and *Abcc8* subunits can be detected in pyramidal cells from wild type mice by scRT-PCR (Figure 3A,B). We next used a dialysis approach by recording neurons with an ATP-free pipette solution (Miki et al., 2001) enriched in sodium (20 mM) to stimulate submembrane ATP depletion and ADP production by the Na^+/K^+ ATPase, which is known to activate K_{ATP} channels (Figure 3H). We confirmed that *Atp1a1* and *Atp1a3* (Figure 3B) were the main α-subunits of the Na^+/K^+ ATPase pump detected in pyramidal neurons (Zeisel et al., 2015;Tasic et al., 2016). Dialysis of ATP-free/20 mM Na^+-pipette solution induced an outward current in most *Kcnj11*$^{+/+}$ neurons recorded (n=19 out of 26; mean for n=26: 46.7 ± 19.0 pA at -50 mV, median value=16.2 pA, Chi^2=5.538, p=0.01860, one sample median test). In some neurons (n=6 of 26), this procedure resulted in an outward current of more than 100 pA that reversed close to E_K (see example in Figure 3C,E). In contrast, this current was not observed in *Kcnj11*$^{-/-}$ neurons ($U_{(26,22)}$=78, p=2.4221 x 10^{-6}, one-tailed, Figure 3D-G). Instead, dialysis induced an inward current in most *Kcnj11*$^{-/-}$ neurons (n=20 of 22; mean for n=22: -59.9 ± 11.9 pA, n=22, median value=-61.9 pA, Chi^2=14.727, p=0.000124, one sample median test), suggesting that other

conductances than the K_{ATP} channels were also altered. Collectively, these data indicate that cortical neurons predominantly express functional K_{ATP} channels composed of KCNJ11 and ABCC8 subunits.

Modulation of neuronal excitability and activity by K_{ATP} channel

Despite their large diversity, cortical neurons display a widespread functional expression of K_{ATP} channels, questioning how these channels integrate the metabolic environment to adjust neuronal activity. To address this question, we first evaluated in identified cortical neurons (n=39) the ability of K_{ATP} channels to modulate neuronal excitability, notably by measuring membrane potentials ($Q_{(2,39)}$=38.000, p=5.6 x 10^{-9}) and membrane resistances ($Q_{(2,39)}$=40.205, p=1.9 x 10^{-9}), as well as spiking activity ($Q_{(2,39)}$=28.593, p=6.2 x 10^{-7}). Following electrophysiological identification, the K_{ATP} channel blocker tolbutamide was applied, which resulted in a slight depolarization (ΔV_m=2.6 ± 0.8 mV, p=1.74 x 10^{-2}, Figure 4A,D) and increase in membrane resistance (ΔR_m=78 ± 32 MΩ, p=1.52 x 10^{-3}, Figure 4B,E). These effects were strong enough to trigger and stimulate the firing of action potentials (ΔF=0.3 ± 0.2 Hz, p= 9.21 x 10^{-3}, Figure 4A,C,F). By contrast, diazoxide hyperpolarized cortical neurons (-4.0 ± 0.6 mV, p=1.87 x 10^{-4}, Figure 4A,D), decreased their membrane resistance (-39 ± 23 MΩ, p=1.52 x 10^{-3}, Figure 4B,E) but did alter their rather silent basal spiking activity (-0.1 ± 0.1 Hz, p=0.821, Figure 4A,C,F).

Most cortical neurons (n=32 of 39) showed modulation of neuronal excitability by both K_{ATP} channel modulators and were considered to be responsive. A similar proportion of responsive neurons was observed between neuronal subtypes (Figure 4-figure supplement 1A, $Chi^2_{(5)}$=7.313, p=0.1984) or groups (Figure 4-figure supplement 1B, p=0.9999, Fisher's exact test). The apparent relative lack of responsiveness in FS-*Pvalb* interneurons (Figure 4-figure supplement 1A), despite a whole-cell K_{ATP} conductance similar to that of other neuronal types (Figure 2-figure supplement 2A), is likely attributable to their low input resistance (Supplementary file 3) making K_{ATP} channels less effective to change membrane potential. Overall, K_{ATP} channels modulated membrane potential, resistance and firing rate by up to 7.9 ± 0.9 mV, 76 ± 17% and 0.5 ± 0.2 Hz, respectively. This modulation of neuronal excitability (Figure 4G-J) and activity (Figure 4-figure supplement 1C,D) was similar between neuronal subtypes or groups (Figure 4H-J and Figure 4-figure supplement 1C-E).

Thus, K_{ATP} channels modulate the excitability and activity of all subtypes of cortical neurons.

Enhancement of neuronal activity by lactate via modulation of K_{ATP} channels

The expression of metabolically sensitive K_{ATP} channels by cortical neurons suggests their ability to couple the local glycolysis capacity of astrocytes with spiking activity. We therefore evaluated whether extracellular changes in glucose and lactate could differentially shape the spiking activity of cortical neurons through their energy metabolism and K_{ATP} channel modulation. Importantly, to preserve intracellular metabolism, neurons were recorded in perforated patch-configuration. Stable firing rates of about 4 Hz inducing ATP consumption by the Na^+/K^+ ATPase (Attwell and Laughlin, 2001) were evoked by applying a depolarizing current and continuously monitored throughout changes in extracellular medium (Figure 5A, $Q_{(2,16)}$=22.625, p=1.222 x 10^{-5}).

Decreasing extracellular glucose from 10 mM to a normoglycemic concentration of 2.5 mM (Silver and Erecinska, 1994;Hu and Wilson, 1997b) did not change firing rate (Figure 5A,B, p=0.2159) of cortical neurons (n=16). By contrast, supplementing extracellular 2.5 mM glucose with 15 mM lactate, an isoenergetic condition to 10 mM glucose for having the same number of carbon atoms, roughly doubled the firing rate compared to both 2.5 (p=7.829 x 10^{-4}) and 10 mM glucose (p=4.303 x 10^{-6}) conditions. Firing rate enhancement by lactate was dose-dependent ($H_{(7,76)}$= 35.142, p= 1.052 x 10^{-5}) and reached statistical significance above 5 mM (Figure 5C). We reasoned that this effect could be mediated by K_{ATP} channel closure. Indeed, the increase in firing rate by lactate (209 ± 49 %) was strongly reduced by the K_{ATP} channel activator diazoxide (71 ± 18 %, p=3.346 x 10^{-3}, Figure 5D). Tolbutamide reversed diazoxide's effect (160 ± 17 %, p=9.345 x 10^{-3}) but did not increase firing rate further (p=0.5076). This occlusion of tolbutamide's effect by 15 mM lactate also suggests that this concentration reaches saturating levels and is the highest metabolic state that can be sensed by K_{ATP} channels. Enhancement of neuronal activity by lactate was also observed in *Kcnj11*$^{+/+}$ cortical neurons (147 ± 25 %, p=2.840 x 10^{-2}) but not in *Kcnj11*$^{-/-}$ mice (112 ± 32 %, p=0.8785, Figure 5E). These observations indicate that lactate enhances neuronal activity via a closure of K_{ATP} channels (Figure 5F).

Mechanism of lactate-sensing

To determine whether lactate-sensing involves intracellular lactate oxidative metabolism and/or extracellular activation of the lactate receptor GPR81, we next probed the expression of monocarboxylate transporters (MCTs), which allow lactate uptake. Consistent with mouse mRNAseq data (Zeisel et al., 2015;Tasic et al., 2016), *Slc16a1* (previously known as MCT1) and *Slc16a7* (previously known as MCT2) were the main transporters detected in rat cortical neurons, although with relatively low single cell detection rates (54 of 277, 19.5% and 78 of 277, 28.2%, for *Slc16a1* and *Slc16a7*, respectively, Figure 6A and Figure 6-figure supplement 1).

The expression of monocarboxylate transporters in cortical neurons is compatible with lactate uptake and metabolism leading to the closure of K_{ATP} channels and an increase in firing rate. We thus evaluated whether lactate uptake was needed for lactate-sensing. We used 250 µM α-cyano-4-hydroxycinnamic acid (4-CIN), a concentration blocking lactate uptake while only moderately altering mitochondrial pyruvate carrier in brain slices (Schurr et al., 1999;Ogawa et al., 2005;Galeffi et al., 2007). 4-CIN reversed the increased firing rate induced by lactate (Figure 6B, $T(9)=0$, $p=7.686 \times 10^{-3}$) indicating that facilitated lactate transport is required for K_{ATP} channel closure and in turn firing rate acceleration.

A mechanism of lactate-sensing involving an intracellular lactate oxidative metabolism would also require the expression of lactate dehydrogenase (LDH), that reversibly converts lactate and nicotinamide adenine dinucleotide (NAD^+) to pyruvate and NADH (Figure 6E, inset). We thus also probed for the expression of *Ldh* subunits. *Ldha* and *Ldhb* were observed in a large majority of cortical neurons with *Ldha* being more frequent in glutamatergic neurons than in GABAergic interneurons ($p=1.61 \times 10^{-2}$, Figure 6A and Figure 6-figure supplement 1). Nonetheless, neuron subtypes analysis did not allow to disclose which populations express less frequently *Ldha*. (Figure 6-figure supplement 1). To confirm the ability of cortical neurons to take up and oxidize lactate we also visualized NADH fluorescence dynamics (Chance et al., 1962) induced by bath application of lactate. Widefield somatic NADH fluorescence appeared as a diffuse labeling surrounding presumptive nuclei (Figure 6D). Consistent with lactate transport by MCTs and oxidization by LDH, NADH was increased under lactate application ($U_{(61,67)}=196$, $p=3.1 \times 10^{-24}$, Figure 6E-F).

Since the lactate receptor GPR81 has been observed in the cerebral cortex (Lauritzen et al., 2014), lactate-sensing might also involve this receptor. This

possibility was ruled out by the observation that pyruvate (15 mM), which is transported by MCTs (Broer et al., 1998;Broer et al., 1999) but does not activate GPR81 (Ahmed et al., 2010), enhanced firing rate to an extent similar to that of lactate (Figure 6C, $U_{(16,6)}$=43, p=0.7468). In line with its uptake and reduction, pyruvate also decreased NADH (Figure 6E-F, $U_{(44,67)}$=868, p=2.08 x 10^{-4}).

The requirement of monocarboxylate transport and the similar effect of lactate and pyruvate on neuronal activity suggest that once taken up, lactate would be oxidized into pyruvate and metabolized by mitochondria to produce ATP, leading in turn to a closure of K_{ATP} channels and increased firing rate. The apparent absence of glucose responsiveness in cortical neurons also suggests that glycolysis contributes modestly to ATP production. To determine the relative contribution of glycolysis and oxidative phosphorylation to ATP synthesis, we transduced the genetically encoded fluorescence resonance energy transfer (FRET)-based ATP biosensor $AT1.03^{YEMK}$ (Imamura et al., 2009) using a recombinant Sindbis virus. $AT1.03^{YEMK}$ fluorescence was mostly observed in pyramidal shaped cells (Figure 6G), consistent with the strong tropism of this viral vector towards pyramidal neurons (Piquet et al., 2018). Blocking glycolysis with 200 µM iodoactic acid (IAA) decreased modestly the FRET ratio by 2.9 ± 0.2% (Figure 6H, p=2.44 x 10^{-13}). By contrast, adding potassium cyanide (KCN, 1mM), a respiratory chain blocker, reduced the FRET ratio to a much larger extent (52.3 ± 0.6%, Figure 6H, p=2.44 x 10^{-13}). KCN also induced a strong NADH fluorescence increase (Figure 6-figure supplement 2A-B, $U_{(12,42)}$=0, p=5.83 x 10^{-12}), indicating a highly active oxidative phosphorylation in cortical neurons.

Discussion

We report that in juvenile rodents extracellular lactate and pyruvate, but not glucose, enhance the activity of cortical neurons through a mechanism involving facilitated transport and the subsequent closure of K_{ATP} channels composed of KCNJ11 and ABCC8 subunits. ATP synthesis derives mostly from oxidative phosphorylation and weakly from glycolysis in cortical neurons. Together with their ability to oxidize lactate by LDH, these observations suggest that lactate is a preferred energy substrate over glucose in cortical neurons. Besides its metabolic importance lactate also appears as a signaling molecule enhancing firing activity (Figure 7). This suggests that an efficient neurovascular and neurometabolic coupling could define a time window of an up state of lactate during which neuronal activity and plasticity would be locally enhanced (Suzuki et al., 2011;Jimenez-Blasco et al., 2020).

K_{ATP} channel subunits in cortical neurons

Similarly to neurons of the hippocampal formation (Zawar et al., 1999;Cunningham et al., 2006;Sada et al., 2015) we found that, regardless of the neuronal type, most neocortical neurons express diazoxide-sensitive, but pinacidil-insensitive K_{ATP} channels (Cao et al., 2009). Since K_{ATP} channel modulators were bath applied, the induced currents recorded from individual cells could also reflect network interactions with neurons and/or astrocytes expressing K_{ATP} channels (Thomzig et al., 2001;Matsumoto et al., 2002). However, the kinetics and reversal potential of the steady state outward currents evoked by K_{ATP} channel modulations do not support an indirect effect induced by transmitter release. In agreement with the observed pharmacological profile (Inagaki et al., 1996) and the absence of functional K_{ATP} channels in *Kcnj11*$^{-/-}$ neurons, we observed that *Kcnj11* and *Abcc8* subunits were the main components of K_{ATP} channels as detected by ribo-tag-based transcriptomics for many neuronal types (Doyle et al., 2008).

Their low detection rate by scRT-PCR is presumably due to the low copy number of their mRNAs, to the low RT efficiency and to the harvesting procedure restricted to the soma. Indeed, a single-cell RNAseq study performed in mouse somatosensory cortex (Zeisel et al., 2015) revealed about 5 molecules of both *Kcnj11* and *Abcc8* mRNAs per cell in cortical neurons, whereas scRT-PCR detection limit was estimated to be around 25 molecules of mRNA in the patch pipette (Tsuzuki et al., 2001). Furthermore, since *Kcnj11* is an intronless gene, collection of the nucleus was

avoided to prevent potential false positives. Thus, neurons positive for both *Kcnj11* and *Sst* intron, taken as an indicator of genomic DNA (Hill et al., 2007;Devienne et al., 2018), were discarded from *Kcnj11* expression analysis. Unavoidably, this procedure does reduce the amount of cytoplasm collected, thereby decreasing the detection rate of both *Kcnj11* and *Abcc8*.

Consistent with the preferred expression of *Kcnj8* in mural and endothelial cells (Bondjers et al., 2006;Zeisel et al., 2015;Tasic et al., 2016;Aziz et al., 2017;Vanlandewijck et al., 2018;Saunders et al., 2018), this subunit was only observed in one out of 277 cortical neurons analyzed. Similarly, SUR2B, the *Abcc9* variant expressed in forebrain (Isomoto et al., 1996) and cortex (Figure 1-figure supplement 1B), whose presence is largely restricted to vascular cells (Zeisel et al., 2015), was not observed in cortical neurons.

Relative sensitivity of cortical neurons to glucose, lactate and pyruvate

Consistent with previous observations (Yang et al., 1999), decreasing extracellular glucose from standard slice concentrations down to a normoglycemic level did not alter firing rates of cortical neurons. However, their activity is silenced during hypoglycemic episodes through K_{ATP} channels activation (Yang et al., 1999;Zawar and Neumcke, 2000;Molnar et al., 2014;Sada et al., 2015). This relative glucose unresponsiveness is in contrast with pancreatic beta cells and hypothalamic glucose-excited neurons whose activity is regulated over a wider range of glucose concentrations by K_{ATP} channels also composed with KCNJ11 and ABCC8 subunits (Aguilar-Bryan et al., 1995;Inagaki et al., 1995a;Miki et al., 1998;Yang et al., 1999;Miki et al., 2001;Tarasov et al., 2006;Varin et al., 2015). The inability of cortical neurons to regulate their spiking activity at glucose levels beyond normoglycemia is likely due to the lack of glucokinase, a hexokinase which catalyzes the first step of glycolysis and acts as a glucose sensor in the millimolar range (German, 1993;Yang et al., 1999). As earlier reported, hexokinase-1 (*Hk1*) is the major isoform in cortical neurons (Zeisel et al., 2015;Tasic et al., 2016;Piquet et al., 2018). Since this enzyme has a micromolar affinity for glucose and is inhibited by its product, glucose-6-phosphate (Wilson, 2003), HK1 is likely already saturated and/or inhibited during normoglycemia thereby limiting glycolysis. Nonetheless, HK1 saturation/inhibition can be mitigated when energy consumption is high (Attwell and Laughlin, 2001;Wilson, 2003;Tantama et al., 2013), and then glucose can probably modulate neuronal

activity via a high affinity mechanism, as evidenced by slow oscillations of spiking activity involving synaptic transmission (Cunningham et al., 2006) or by the use of glucose-free whole-cell patch-clamp solution (Kawamura, Jr. et al., 2010) that mimics high glucose consumption (Piquet et al., 2018;Diaz-Garcia et al., 2019).

Similarly to glucose-excited hypothalamic neurons (Yang et al., 1999;Song and Routh, 2005), but in contrast with pancreatic beta cells (Newgard and McGarry, 1995), cortical neurons were dose-dependently excited by lactate. This lactate sensitivity is consistent with lactate transport and oxidization in hypothalamic and cortical neurons (Ainscow et al., 2002;Sada et al., 2015;Diaz-Garcia et al., 2017) which are low in beta cells (Sekine et al., 1994;Pullen et al., 2011). Pyruvate had a similar effect to lactate in cortical neurons under normoglycemic condition whereas it only maintains the activity of hypothalamic glucose-excited neurons during hypoglycemia (Yang et al., 1999) and barely activates pancreatic beta cells (Dufer et al., 2002). Thus, cortical neurons display a peculiar metabolic sensitivity to monocarboxylates. Our data also suggest that under normoglycemic conditions a portion of K_{ATP} channels are open when cortical neurons fire action potentials.

Mechanism of lactate-sensing

Our pharmacological, molecular and genetic evidence indicates that the closure of K_{ATP} channels is responsible for the firing rate enhancement by lactate. Since K_{ATP} channels can be modulated by G protein-coupled receptors (Kawamura, Jr. et al., 2010), lactate-sensing might have been mediated by GPR81, a G_i protein-coupled lactate receptor expressed in the cerebral cortex (Lauritzen et al., 2014). This possibility is however unlikely since the activation of GPR81 inhibits cultured cortical neurons (Bozzo et al., 2013;de Castro Abrantes H. et al., 2019) and we show here that enhancing effect pyruvate on neuronal activity was similar to that of lactate, although pyruvate does not activate GPR81 (Ahmed et al., 2010).

We found that lactate-sensing was critically dependent on lactate transport and we confirmed the capacity of cortical neurons to take up and oxidize lactate (Bittar et al., 1996;Laughton et al., 2000;Bouzier-Sore et al., 2003;Wyss et al., 2011;Choi et al., 2012;Sada et al., 2015;Machler et al., 2016). Although *Slc16a1* and *Slc16a7* mRNAs were infrequently detected by scRT-PCR, our imaging and electrophysiological observations indicate a widespread transport of lactate. Similarly to K_{ATP} channel

subunits, the relatively low single cell detection rates are likely due to the low copy number of both *Slc16a1* and *Slc16a7* mRNAs which have been reported to be less than 10 copies per cell in cortical neurons (Zeisel et al., 2015). Interestingly, discrepancies between mRNA and protein expression have been reported for MCTs (Pierre and Pellerin, 2005) which may reflect regulation at the translational level and/or a low turnover of the proteins. The ability of cortical neurons to oxidize lactate is supported by both scRT-PCR and NADH imaging observations. The much higher detection rates of *Ldha* and *Ldhb* mRNA parallel their single cell copy number which is two to five times higher than that of *Ldha* and *Ldhb* (Zeisel et al., 2015).

The impairment of lactate-enhanced firing by 4-CIN might be due to the blockade of lactate uptake by neurons but also to the blockade of lactate efflux by astrocytes. However, it is unlikely that astrocytes have a substantial contribution here. First, basal lactate tone in cortical slices has been estimated to be about 200 µM (Karagiannis et al., 2015), a concentration with little or no effect on lactate-sensing (Figure 5C). Second, in addition to MCTs, astrocytes can also release lactate from connexin hemichannels (Karagiannis et al., 2015) and from a lactate-permeable ion channel (Sotelo-Hitschfeld et al., 2015). Hence, blockade of MCTs by 4-CIN would have, at most, only partially altered the release of lactate by astrocytes.

LDH metabolites, including pyruvate and oxaloacetate, can lead to K_{ATP} channel closure (Dhar-Chowdhury et al., 2005;Sada et al., 2015) and could mediate lactate-sensing. An intermediate role of oxaloacetate in lactate-sensing is compatible with enhanced Krebs cycle and oxidative phosphorylation, which leads to an increased ATP/ADP ratio and the closure of K_{ATP} channels (Figure 7). In contrast to oxaloacetate, intracellular ATP was found to be ineffective for reverting K_{ATP} channel opening induced by LDH inhibition (Sada et al., 2015). Interestingly, hippocampal interneurons were found to be insensitive to glucose deprivation in whole cell configuration (Sada et al., 2015) but not in perforated patch configuration (Zawar and Neumcke, 2000) whereas almost the opposite was found in CA1 pyramidal cells. Whether altered intracellular metabolism by whole-cell recording accounted for the apparent lack of ATP sensitivity remains to be determined.

Increased firing rate by lactate metabolism is likely to enhance sodium influx and stimulate ATP comsumption by the Na^+/K^+ ATPase (Tanner et al., 2011). This could in turn lower ATP/ADP ratio, increase the P_0 of K_{ATP} channels (Tantama et al., 2013) and subsequently decrease firing rate. We did not observe such a decrease and,

once firing rate was enhanced, it remained stable for several minutes (Figure 5A). This suggests that ATP levels remained relatively stable, as reported in pancreatic cells under high glucose stimulation that recruits calcium dependent energy metabolism (Tanaka et al., 2014). However, when energy consumption is high, as during network synaptic transmission, fluctuations of ATP/ADP ratio and slow oscillations of spiking activity can occur as observed in the entorhinal cortex (Cunningham et al., 2006).

Lactate as an energy substrate for neurons and an enhancer of spiking activity and neuronal plasticity

We confirmed that the ATP produced by cortical neurons was mostly derived from oxidative phosphorylation and marginally from glycolysis (Almeida et al., 2001;Hall et al., 2012). Together with the enhancement of spiking activity through K_{ATP} channels by lactate, but not by glucose, our data support both the notion that lactate is a preferred energy substrate over glucose for neonatal and juvenile cortical neurons (Bouzier-Sore et al., 2003;Ivanov et al., 2011) as well as the astrocyte-neuron lactate shuttle hypothesis (Pellerin and Magistretti, 1994). Whether lactate-sensing persists in the adult remains to be determined.

Although the local cellular origin of lactate has been recently questioned (Lee et al., 2012;Diaz-Garcia et al., 2017), a growing number of evidence indicates that astrocytes are major central lactate producers (Almeida et al., 2001;Choi et al., 2012;Sotelo-Hitschfeld et al., 2015;Karagiannis et al., 2015;Le Douce J. et al., 2020;Jimenez-Blasco et al., 2020).

Glutamatergic synaptic transmission stimulates blood glucose uptake, astrocyte glycolysis, as well as lactate release (Pellerin and Magistretti, 1994;Voutsinos-Porche et al., 2003;Ruminot et al., 2011;Choi et al., 2012;Sotelo-Hitschfeld et al., 2015;Lerchundi et al., 2015) and diffusion through the astroglial gap junctional network (Rouach et al., 2008). This indicates that local and fast glutamatergic synaptic activity would be translated by astrocyte metabolism into a widespread and long-lasting extracellular lactate increase (Prichard et al., 1991;Hu and Wilson, 1997a), which could in turn enhance the firing of both excitatory and inhibitory neurons (Figure 7). Such a lactate surge would be spatially confined by the gap junctionnal connectivity of the astroglial network, which in layer IV represents an entire barrel (Houades et al., 2008).

This suggests that increased astrocytic lactate induced by whisker stimulation could enhance the activity of the cortical network and fine-tune upcoming sensory processing for several minutes, thereby favoring neuronal plasticity. Along this line, lactate derived from astrocyte glycogen supports both neuronal activity and long-term memory formation (Suzuki et al., 2011;Choi et al., 2012;Vezzoli et al., 2020). Similarly, cannabinoids, which notably alter neuronal processing and memory formation (Stella et al., 1997), hamper lactate production by astrocytes (Jimenez-Blasco et al., 2020).

In contrast to glucose levels, lactate levels are higher in extracellular fluid than in plasma and can be as high as 5 mM under basal resting condition (Abi-Saab et al., 2002;Zilberter et al., 2010). Given that extracellular lactate is almost doubled during neuronal activity (Prichard et al., 1991;Hu and Wilson, 1997a), enhancement of neuronal activity by lactate is likely to occur when the brain is active. Peripheral lactate released by skeletal muscles, which can reach 15 mM in plasma following an intense physical exercise (Quistorff et al., 2008), could also facilitate this effect. Although systemic increase of lactate elevates its cerebral extracellular concentration (Machler et al., 2016;Carrard et al., 2018) to a level with little or no effect on firing rate, when both the brain and the body are active, as during physical exercise, both astrocytes and systemic lactate could contribute to enhance spiking activity.

Blood-borne lactate has been shown to promote learning and memory formation via brain-derived neurotrophic factor (El Hayek L. et al., 2019). It is worth noting that the production of this neurotrophin is altered in *Kcnj11*$^{-/-}$ mice and impaired by a K_{ATP} channel opener (Fan et al., 2016), both conditions compromising the effect of lactate on spiking activity. Hence, the increase in astrocyte and systemic lactate could fine-tune neuronal processing and plasticity in a context-dependent manner and their coincidence could be potentially synergistic.

Lactate-sensing compensatory mechanisms

Since excitatory neuronal activity increases extracellular lactate (Prichard et al., 1991;Hu and Wilson, 1997a) and lactate enhances neuronal activity, such a positive feedback loop (Figure 7) suggests that compensatory mechanisms might be recruited to prevent an overexcitation of neuronal activity by lactate supply. A metabolic negative feedback mechanism could involve the impairment of astrocyte

metabolism and lactate release by endocannabinoids (Jimenez-Blasco et al., 2020) produced during intense neuronal activity (Stella et al., 1997).

Another possibility would consist in a blood flow decrease that would in turn reduce the delivery of blood glucose and subsequent local lactate production and release but also blood-borne lactate. Some GABAergic interneuron subtypes (Cauli et al., 2004;Uhlirova et al., 2016;Krawchuk et al., 2019), but also astrocytes (Girouard et al., 2010), can trigger vasoconstriction and blood flow decrease when their activity is increased. This could provide a negative hemodynamic feedback restricting spatially and temporally the increase of spiking activity by lactate.

PVALB-expressing and SST-expressing interneurons exhibit higher mitochondrial content and apparent oxidative phosphorylation than pyramidal cells (Gulyas et al., 2006) suggesting that interneurons would more rapidly metabolize and sense lactate than pyramidal cells. These inhibitory GABAergic interneurons might therefore silence the cortical network, thereby providing a negative neuronal feedback loop. Active decrease in blood flow is associated with a decrease in neuronal activity (Shmuel et al., 2002;Shmuel et al., 2006;Devor et al., 2007). Vasoconstrictive GABAergic interneurons may underlie for both processes and could contribute to returning the system to a low lactate state.

Conclusion

Our data indicate that lactate is both an energy substrate for cortical neurons and a signaling molecule enhancing their spiking activity. This suggests that a coordinated neurovascular and neurometabolic coupling would define a time window of an up state of lactate that, besides providing energy and maintenance to the cortical network, would fine-tune neuronal processing and favor, for example, memory formation (Suzuki et al., 2011;Kann et al., 2014;Galow et al., 2014;Jimenez-Blasco et al., 2020).

Acknowledgments

This work was supported by grants from the Human Frontier Science Program (HFSP, RGY0070/2007, BC), the Agence Nationale pour la Recherche (ANR 2011 MALZ 003 01, BC). AK was supported by a Fondation pour la Recherche Médicale fellowship (FDT20100920106). BLG was supported by a Fondation pour la

Recherche sur Alzheimer fellowship. We thank the animal facility of the IBPS (Paris, France).

Competing interests

The authors declare no competing interests.

Materials and methods

Lead contact and materials availability

Further information and requests for resources and reagents should be directed to, and will be fulfilled by, the lead contact, B. Cauli (bruno.cauli@upmc.fr).

Experimental model and subject details

Wistar rats, C57BL/6RJ or *Kcnj11*$^{-/-}$ (B6.129P2-*Kcnj11*^{tm1Sse}, backcrossed into C57BL6 over six generations) mice were used for all experiments in accordance with French regulations (Code Rural R214/87 to R214/130) and conformed to the ethical guidelines of both the directive 2010/63/EU of the European Parliament and of the Council and the French National Charter on the ethics of animal experimentation. A maximum of 3 rats or 5 mice were housed per cage and single animal housing was avoided. Male rats and mice of both genders were housed on a 12-hour light/dark cycle in a temperature-controlled (21–25°C) room and were given food and water *ad libitum.* Animals were used for experimentation at 13-24 days of age.

Cortical slice preparation

Rats or mice were deeply anesthetized with isoflurane. After decapitation brains were quickly removed and placed into cold (~4°C) oxygenated artificial cerebrospinal fluid (aCSF) containing (in mM): 126 NaCl, 2.5 KCl, 1.25 NaH_2PO_4, 2 $CaCl_2$, 1 $MgCl_2$, 26 $NaHCO_3$, 10 glucose, 15 sucrose, and 1 kynurenic acid. Coronal slices (300 µm thick) containing the barrel cortex were cut with a vibratome (VT1000S, Leica) and allowed to recover at room temperature for at least 1h in aCSF saturated with O_2/CO_2 (95 %/5 %) as previously described (Karagiannis et al., 2009;Devienne et al., 2018).

Whole-cell patch-clamp recording

Patch pipettes (4-6 MΩ) pulled from borosilicate glass were filled with 8 µl of RNAse free internal solution containing in (mM): 144 K-gluconate, 3 $MgCl_2$, 0.5 EGTA, 10

HEPES, pH 7.2 (285/295 mOsm). Whole-cell recordings were performed at 25.3 ± 0.2°C using a patch-clamp amplifier (Axopatch 200B, Molecular Devices). Data were filtered at 5-10 kHz and digitized at 50 kHz using an acquisition board (Digidata 1440, Molecular Devices) attached to a personal computer running pCLAMP 10.2 software package (Molecular Devices). For ATP washout experiments neurons were recorded in voltage clamp mode using an ATP-free internal solution containing in (mM): 140 KCl, 20 NaCl, 2 $MgCl_2$, 10 EGTA, 10 HEPES, pH 7.2.

Cytoplasm harvesting and scRT-PCR

At the end of the whole-cell recording, lasting less than 15 min, the cytoplasmic content was aspirated in the recording pipette. The pipette's content was expelled into a test tube and reverse transcription (RT) was performed in a final volume of 10 µl, as described previously (Lambolez et al., 1992). The scRT-PCR protocol was designed to probe simultaneously the expression of neuronal markers, K_{ATP} channels subunits or some key elements of lactate metabolism. Two-steps amplification was performed essentially as described (Cauli et al., 1997;Devienne et al., 2018). Briefly, cDNAs present in the 10 µl reverse transcription reaction were first amplified simultaneously using all external primer pairs listed in the Key Ressources Table. Taq polymerase and 20 pmol of each primer were added to the buffer supplied by the manufacturer (final volume, 100 µl), and 20 cycles (94°C, 30 s; 60°C, 30 s; 72°C, 35 s) of PCR were run. Second rounds of PCR were performed using 1 µl of the first PCR product as a template. In this second round, each cDNA was amplified individually using its specific nested primer pair (Key Ressources Table in Appendix) by performing 35 PCR cycles (as described above). 10 µl of each individual PCR product were run on a 2 % agarose gel stained with ethidium bromide using ΦX174 digested by *Hae*III as a molecular weight marker.

Perforated patch-clamp recording

Gramicidin stock solution (2 mg/ml, Sigma-Aldrich) was prepared in DMSO and diluted to 10-20 µg/ml (Zawar and Neumcke, 2000) in the RNAse free internal solution described above. The pipette tip was filled with gramicidin-free solution. Progress in perforation was evaluated by monitoring the capacitive transient currents elicited by -10 mV voltage pulses from a holding potential of -60 mV. In perforated patch configuration, a continuous current (52 ± 7 pA) was injected to induce the

spiking of action potentials at stable firing rates of 4.1 ± 0.4 Hz obtained after an equilibration period of 3.6 ± 0.5 min. Membrane and access resistance were continuously monitored by applying -50 pA hyperpolarizing current pulses lasting 1 s every 10 s using an external stimulator (S900, Dagan) connected to the amplifier. Recordings were stopped when going into whole-cell configuration occurred, as evidenced by sudden increase of spike amplitude and decrease of access resistance.

NADH imaging

Recordings were made in layer II-III of the rat somatosensory cortex. Wide-field fluorescent images were obtained using a double port upright microscope BX51WI, WI-DPMC, Olympus) with a 60x objective (LUMPlan Fl /IR 60x/0.90 W, Olympus) and a digital camera (CoolSnap HQ2, Roper Scientific) attached on the front port of the microscope. NADH autofluorescence was obtained by 365 nm excitation with a Light Emitting Device (LED, pE-2, CoolLED) using Imaging Workbench 6.0.25 software (INDEC Systems) and dichroic (FF395/495/610-Di01-25x36, Semrock) and emission filters (FF01-425/527/685-25, Semrock). Infrared Dodt gradient contrast images (IR-DGC, (Dodt and Zieglgansberger, 1998)) were obtained using a 780 nm collimated LED (M780L3-C1,Thorlabs) as a transmitted light source and DGC optics (Luigs and Neumann). Autofluorescence and IR-DGC images were collected every 10s by alternating the fluorescence and transmitted light sources. In parallel, infrared transmitted light images of slices were also continuously monitored on the back-port of the microscope using a customized beam splitter (725 DCSPXR, Semrock) and an analogic CCD camera (XC ST-70 CE, Sony). The focal plane was maintained constant on-line using infrared DGC images of cells as anatomical landmarks (Lacroix et al., 2015).

Subcloning and viral production

The coding sequence of the ATP sensor ATeam1.03YEMK (Imamura et al., 2009) was subcloned into the viral vector pSinRep5. Sindbis virus was produced as previously described (Piquet et al., 2018). Recombinant pSinRep5 and helper plasmid pDH26S (Invitrogen) were transcribed in vitro into capped RNA using the Megascript SP6 kit (Ambion). Baby hamster kidney-21 cells (BHK-21, clone 13, *Mesocricetus auratus*, hamster, Syrian golden), negative for mycoplasma

contamination and purchased from ATCC (CCL-10, RRID:CVCL_1915, lot number 1545545), were only used for viral production. BHK-21 cells were electroporated with sensor-containing RNA and helper RNA (2.10^7 cells, 950 µF, 230 V) and incubated for 24 h at 37°C in 5% CO_2 in Dulbecco's modified Eagle Medium supplemented with 5% fetal calf serum before collecting cell supernatant containing the viruses. The virus titer (10^8 infectious particles/ml) was determined after counting fluorescent baby hamster kidney cells infected using serial dilution of the stock virus.

Brain slice viral transduction

Brain slices were placed onto a millicell membrane (Millipore) with culture medium (50% minimum essential medium, 50% Hank's balanced salt sodium, 6.5 g/l glucose and 100 U/ml penicillin-streptomycin (Sigma-Aldrich) as previously described (Piquet et al., 2018). Infection was performed by adding ~5 x 10^5 particles per slice. Slices were incubated overnight at 35°C in 5% CO2. The next morning, brain slices were equilibrated for 1h in aCSF containing (in mM): 126 NaCl, 2.5 KCl, 1.25 NaH_2PO_4, 2 $CaCl_2$, 1 $MgCl_2$, 26 $NaHCO_3$, 10 glucose, 15 sucrose. Slices were then placed into the recording chamber, heated at ~30 °C and continuously perfused at 1-2 ml/min.

FRET imaging

Recordings were made from visually identified pyramidal cells in layer II-III of the rat somatosensory cortex. Wide-field fluorescent images were obtained using a 40x objective and a digital camera attached on the front port of the microscope. The ATP sensor ATeam1.03YEMK was excited at 400 nm with a LED using Imaging Workbench 6.0.25 software and excitation (FF02-438/24-25, Semrock) and dichroic filters (FF458-Di02-25x36, Semrock). Double fluorescence images were collected every 15s by alternating the fluorescence emission filters for the CFP (FF01-483/32-25, Semrock) and the YFP (FF01-542/27-25, Semrock) using a filter wheel (Lambda 10B, Sutter Instruments). The focal plane was maintained constant on-line as described above.

Pharmacological studies

Pinacidil (100 µM, Sigma-Aldrich); Diazoxide (300 µM, Sigma-Aldrich) and Tolbutamide (500 µM, Sigma-Aldrich), Mn(III)tetrakis(1-methyl-4-pyridyl)porphyrin (MnTMPyP, 25 µM, Millipore), α-cyano-4-hydroxycinnamate (4-CIN, 250 µM, Sigma-

Aldrich); iodoacetic acid (IAA, 200 µM, Sigma-Aldrich) or KCN (1 mM, Sigma-Aldrich) was dissolved in aCSF from stock solutions of pinacidil (100 mM; NaOH 1M), diazoxide (300 mM; NaOH 1M), tolbutamide (500 mM; NaOH 1M), 4-CIN (250 mM; DMSO), IAA (200 mM, water) and KCN (1 M, water). Changes in extracellular glucose, lactate or pyruvate concentration were compensated by changes in sucrose concentration to maintain the osmolarity of the aCSF constant as previously described (Miki et al., 2001;Varin et al., 2015;Piquet et al., 2018) and pH was adjusted to 7.4.

Quantification and statistical analysis

Analysis of somatic features

The laminar location determined by infrared videomicroscopy and recorded as 1-4 according to a location right within layers I, II/III or IV. For neurons located at the border of layers I-II/III and II/III-IV, the laminar location was represented by 1.5 and 3.5, respectively. Somatic features were measured from IR DGC of the recorded neurons. Briefly, the soma was manually delineated using Image-Pro Analyzer 7.0 software (MediaCybernetics) and length of major and minor axes, perimeter and area were extracted. The soma elongation was calculated as the ratio between major and minor axis. Roundness was calculated according to: $\frac{perimeter^2}{4\pi \times area}$; a value close to 1 is indicative of round somata.

Analysis of electrophysiological properties

32 electrophysiological properties chosen to describe the electrophysiological diversity of cortical neurons (Ascoli et al., 2008) were determined using the I-clamp fast mode of the amplifier as previously described (Karagiannis et al., 2009). Membrane potential values were corrected for theoretical liquid junction potential (-15.6 mV). Resting membrane potential was measured just after passing in whole-cell configuration, and only cells with a resting membrane potential more negative than -55 mV were analyzed further. Membrane resistance (R_m) and membrane time constant (τ_m) were determined on responses to hyperpolarizing current pulses (duration, 800 ms) eliciting voltage shifts of 10-15 mV negative to rest (Kawaguchi, 1993;Kawaguchi, 1995). Time constant was determined by fitting this voltage

response to a single exponential. Membrane capacitance (C_m) was calculated according to $C_m=\tau_m/R_m$. Sag index was quantified as a relative decrease in membrane conductance according to $(G_{sag}-G_{hyp})/G_{sag}$ (Halabisky et al., 2006) where G_{hyp} and G_{sag} correspond to the whole-cell conductance when the sag was inactive and active, respectively. G_{sag} was measured as the slope of the linear portion of a current–voltage (I–V) plot, where V was determined at the end of 800 ms hyperpolarizing current pulses (-100 to 0 pA) and G_{hyp} as the slope of the linear portion of an I–V plot, where V was determined as the maximal negative potential during the 800 ms hyperpolarizing pulses. Rheobase was quantified as the minimal depolarizing current pulse intensity (800 ms duration pulses, 10 pA increments) generating at least one action potential. First spike latency (Gupta et al., 2000;Ascoli et al., 2008) was measured at rheobase as the time needed to elicit the first action potential. To describe different firing behaviors near threshold, spike frequency was measured near spike threshold on the first trace in which at least three spikes were triggered. Instantaneous discharge frequencies were measured and fitted to a straight line according to $F_{threshold} = m_{threshold}.t + F_{min.}$, where $m_{threshold}$ is the slope termed adaptation, t the time and F_{min}, the minimal steady state frequency. Analysis of the action potentials waveforms was done on the first two spikes. Their amplitude (A1 and A2) was measured from threshold to the positive peak of the spike. Their duration (D1 and D2) was measured at half amplitude (Kawaguchi, 1993;Cauli et al., 1997). Their amplitude reduction and the duration increase were calculated according to (A1-A2)/A1 and (D2-D1)/D1, respectively (Cauli et al., 1997;Cauli et al., 2000). The amplitude and the latency of the fast and medium afterhyperpolarization (fAH and mAH) were measured for the first two action potentials as the difference between spike threshold and the negative peak of the AHs (Kawaguchi, 1993). The amplitude and latency of afterdepolarization (AD) following single spikes (Haj-Dahmane and Andrade, 1997) were measured as the difference between the negative peak of the fAH and the peak of the AD and between the spike threshold and the peak of the AD, respectively. When neurons did not exhibit mAH or AD, amplitude and latency were arbitrarily set to 0. A complex spike amplitude accommodation during a train of action potentials, consisting in a transient decrease of spikes amplitude, was measured as the difference between the peak of the smallest action potential and the peak of the following largest action potential (Cauli et al., 2000). Maximal firing rate was defined as the last trace before prominent

reduction of action potentials amplitude indicative of a saturated discharge. To take into account the biphasic spike frequency adaptation (early and late) occurring at high firing rates (Cauli et al., 1997;Cauli et al., 2000;Gallopin et al., 2006), instantaneous firing frequency was fitted to a single exponential (Halabisky et al., 2006) with a sloping baseline, according to : $F_{Saturation} = A_{sat}.e^{-t/\tau_{sat}} + t.m_{sat} + F_{max}$, where A_{sat} corresponds to the amplitude of early frequency adaptation, τ_{sat} to the time constant of early adaptation, m_{sat} to the slope of late adaptation and F_{max} to the maximal steady state frequency.

Unsupervised clustering

To classify neurons unsupervised clustering was performed using the laminar location of the soma, 10 molecular parameters (*Slc17a7*, *Gad2* and/or *Gad1*, *Nos1*, *Calb1*, *Pvalb*, *Calb2*, *Npy*, *Vip*, *Sst* and *Cck*) and the 32 electrophysiological parameters described above. Neurons positive for *Gad2* and/or *Gad1* were denoted as *Gad* positive and these mRNAs were considered as a single molecular variable as previously described (Gallopin et al., 2006). Parameters were standardized by centering and reducing all of the values. Cluster analysis was run on Statistica 6.1 software (Statsoft) using Ward's method (Ward, 1963). The final number of clusters was established by hierarchically subdividing the clustering tree into higher order clusters as previously described (Karagiannis et al., 2009).

Analysis of voltage clamp recordings

Whole-cell currents were measured from a holding potential of -70 mV and membrane resistances were determined by applying a voltage step to -60 mV of 100 ms every 5 s. The effects of K_{ATP} channel modulators were measured at the end of drug application by averaging, over a period of 1 minute, whole cell currents and changes in membrane resistance relative to control baseline prior to the application of drugs. Whole-cell K_{ATP} current and conductance were determined by subtracting current and conductance measured under K_{ATP} channel activator by their value measured under K_{ATP} channel blocker. The relative whole-cell K_{ATP} conductance was determined by dividing the whole-cell K_{ATP} conductance by the whole cell conductance measured under K_{ATP} channel activator. Whole-cell K_{ATP} current density

was determined by dividing the whole-cell K_{ATP} current by the membrane capacitance. K_{ATP} current reversal potential was measured by subtracting I/V relationships obtained during voltage ramps from -60 to -130 mV determined under K_{ATP} channel activator and blocker, respectively.

During ATP washout experiments, whole-cell currents and I/V relationships were measured every 10 s at a holding potential of -50 mV and during voltage ramps from -40 to -120 mV, respectively. Washout currents were determined by subtracting the whole-cell currents measured at the beginning and the end of the whole cell-recording, respectively.

Analysis of current clamp recordings

Every 10 s, membrane potential and mean firing rate were measured and membrane resistances were determined from voltage responses induced by -50 pA currents pulses lasting 1 s. K_{ATP} voltage response and changes in membrane resistance and firing rate were determined by subtracting their value measured under K_{ATP} channel activator by their value measured under K_{ATP} channel blocker. Neurons were considered as responsive to K_{ATP} channel modulators if the K_{ATP} channel activator induced both a hyperpolarization and a decrease in membrane resistance reversed by the K_{ATP} channel blocker.

Analysis of perforated patch recordings

Mean firing frequency was measured every 10 s. Quantification of spiking activity was determined by averaging firing frequency over a period of 5 min preceding a change in extracellular aCSF composition. Firing frequencies were normalized by the averaged mean firing frequency measured under control condition.

NADH imaging

Shading correction was applied off-line on the NADH autofluorescence images using the "Shading Corrector" plugin of FIJI software (Schindelin et al., 2012) and a blank field reference image. To compensate for potential x-y drifts all IR-DGC images were realigned off-line using the "StackReg" and "TurboReg" plugins (Thevenaz et al., 1998) of FIJI software and the same registration was applied to the corrected NADH autofluorescence images. To determine somatic regions of interest (ROIs) the soma was manually delineated on IR-DGC images. The mean NADH autofluorescence

was measured at each time point using the same ROIs. Variations of fluorescence intensity were expressed as the ratio (F-F0)/F0 where F corresponds to the mean fluorescence intensity in the ROI at a given time point, and F0 corresponds to the mean fluorescence intensity in the same ROI during the 5 min control baseline prior to changes in aCSF composition. Effect of monocarboxylate superfusion or oxidative phosphorylation blockade was quantified by averaging the normalized ratio (R/R0) during the last five minutes of drug application.

FRET imaging

All images were realigned off-line as described above using the YFP images as the reference for registration. Fluorescence ratios were calculated by dividing the registered YFP images by the registered CFP images using FIJI. The somatic ROIs were manually delineated on the YFP images as described above. The mean ratio was measured at each time point using the same ROIs. Variations of fluorescence ratio were expressed as the ratio (R-R0)/R0 where R corresponds to the fluorescence ratio in the ROI at a given time point, and R0 corresponds to the mean fluorescence ratio in the same ROI during the 10 min control baseline prior to drug application. Effect of glycolysis or oxidative phosphorylation blockade was quantified by averaging the normalized ratio during the last five minutes of drug application.

Statistical analysis

Statistical analyses were performed with Statistica 6.1 and GraphPad Prism 7. All values are expressed as means ± s.e.m. Normality of distributions and equality of variances were assessed using the Shapiro–Wilk test and the Fisher F-test, respectively. Parametric tests were only used if these criteria were met. Holm-Bonferroni correction was used for multiple comparisons and p-values are given as uncorrected. Statistical significance on all figures uses the following convention of corrected p-values: * $p < 0.05$, ** $p < 0.01$, *** $p < 0.001$.

Statistical significance of morphological and electrophysiological properties of neurons was determined using the Mann-Withney U test. Comparison of the occurrence of expressed genes and of responsiveness of K_{ATP} channel modulators between different cell types was determined using Fisher's exact test. Statistical significance of the effects of K_{ATP} channel modulators was determined using the Friedman and post hoc Dunn's tests. Significance of the effect of the ROS scavenger

was determined using one-tailed unpaired student t-test. Comparison of K_{ATP} channel properties was determined using Mann-Withney U, Student-t, or Kruskal-Wallis H tests. Comparison of responses between *Kcnj11*$^{+/+}$ and *Kcnj11*$^{-/-}$ neurons was determined using Mann-Withney U test. Statistical significance of the effects of energy substrates and drug applications on evoked firing in perforated patch recordings was determined using Friedman and Dunn's tests. Comparison of the effects of monocarboxylates and cyanide on NADH fluorescence was determined using Mann-Withney U test. Statistical significance of the effects of metabolic inhibitors on intracellular ATP was determined using Friedman and Dunn's tests.

Figure legends

Figure 1. Detection of *Kcnj11* and *Abcc8* K_{ATP} channel subunits in cortical neuron subtypes.

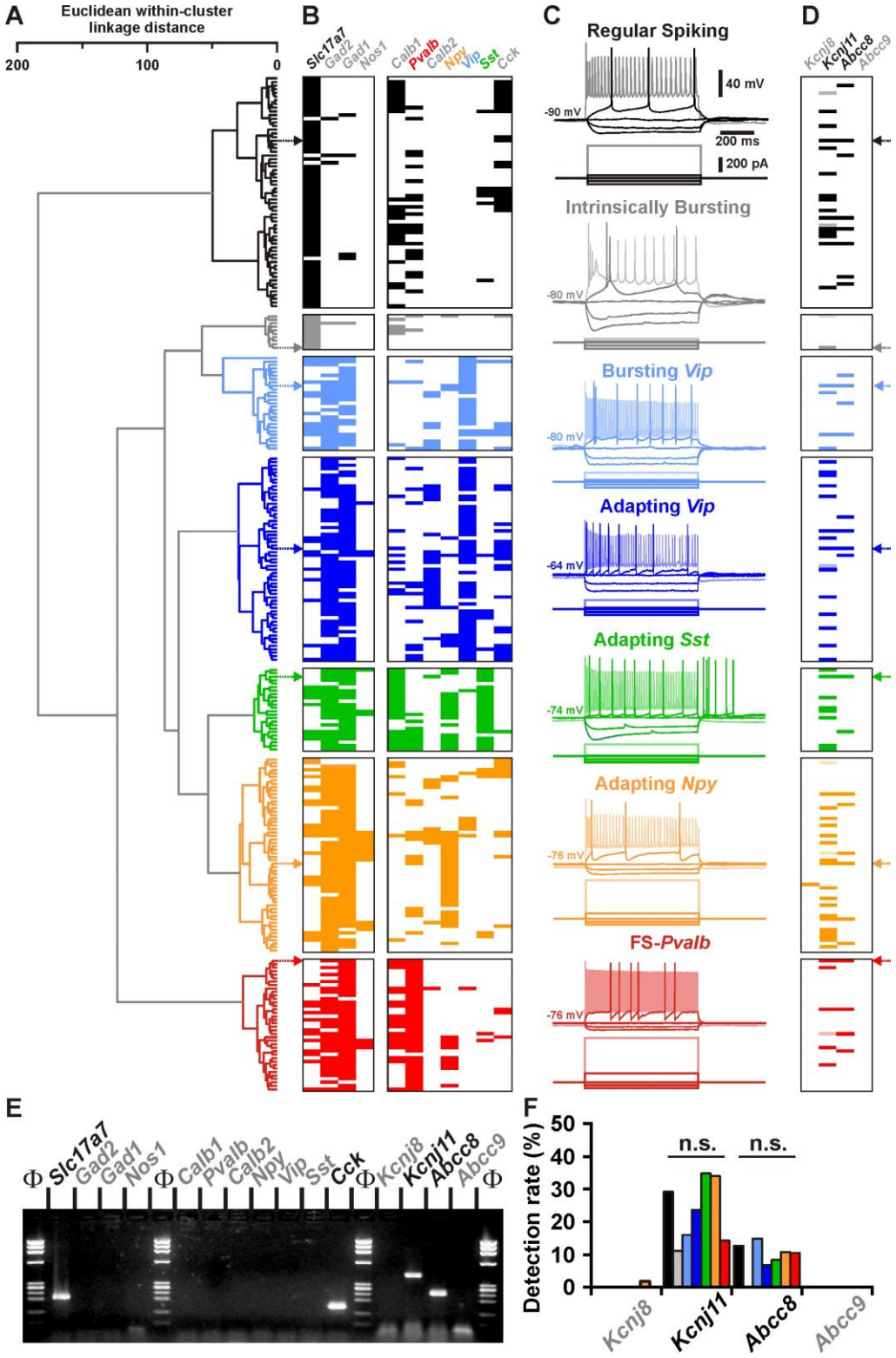

(A) Ward's clustering of 277 cortical neurons (left panel). The x axis represents the average within-cluster linkage distance, and the y axis the individuals.
(B) Gene detection profile across the different cell clusters. For each cell, colored and white rectangles indicate presence and absence of genes, respectively. (C) Representative voltage responses induced by injection of current pulses (bottom traces) corresponding to -100, -50 and 0 pA, rheobase and intensity inducing a saturating firing frequency (shaded traces) of a Regular Spiking neuron (black), an Intrinsically Bursting neuron (gray), a Bursting *Vip* interneuron (light blue), an Adapting *Vip* interneuron (blue), an Adapting *Sst* interneuron (green), an Adapting *Npy* interneuron (orange), and a Fast Spiking-Parvalbumin interneuron (FS-*Pvalb*, red). The colored arrows indicate the expression profiles of neurons whose firing pattern is illustrated in (C).
(D) Detection of the subunits of the K_{ATP} channels in the different clusters. Shaded rectangles represent potential *Kcnj11* false positives in which genomic DNA was detected in the harvested material.
(E) scRT-PCR analysis of the RS neuron depicted in (A-D).
(F) Histograms summarizing the detection rate of K_{ATP} channel subunits in identified neuronal types. n.s. not statistically significant.

Figure 1-figure supplement 1. Molecular expression of K_{ATP} channels.

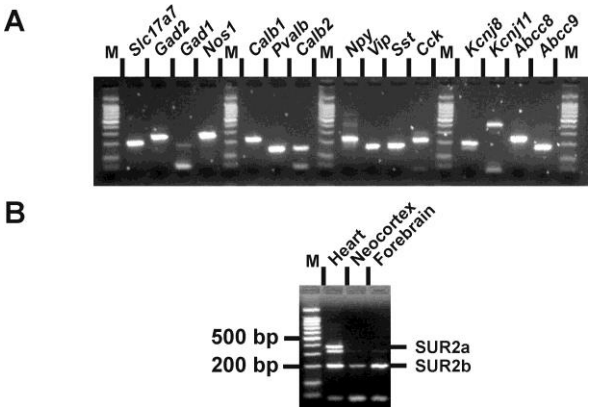

(A) RT-PCR products generated from 500 pg of total cortical RNAs. M: 100 bp ladder molecular weight marker.
(B) *Abcc9* splice variants-specific RT-PCR analysis of 1 ng total RNAs from rat heart, neocortex and forebrain.

Figure 2. Pharmacological and biophysical characterization of K_{ATP} channels in cortical neurons.

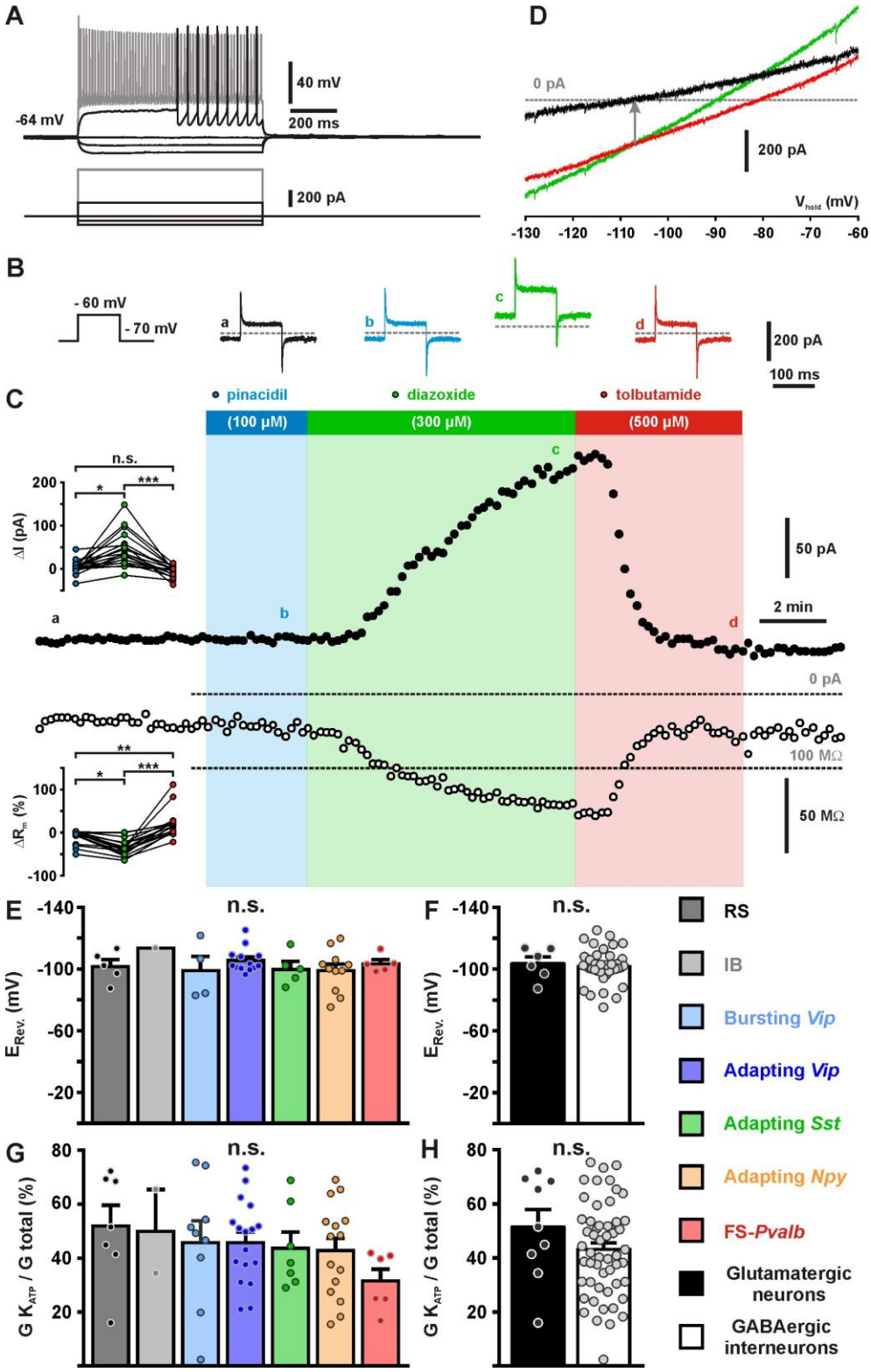

(A) Representative voltage responses of a FS-*Pvalb* interneuron induced by injection of current pulses (bottom traces).
(B) Protocol of voltage pulses from −70 to −60 mV (left trace). Responses of whole-cell currents in the FS-*Pvalb* interneurons shown in (A) in control condition (black) and in presence of pinacidil (blue), piazoxide (green) and tolbutamide (red) at the time indicated by a-d in (C).
(C) Stationary currents recorded at -60 mV (filled circles) and membrane resistance (open circles) changes induced by K_{ATP} channel modulators. The colored bars and shaded zones indicate the duration of application of K_{ATP} channel modulators. Upper and lower insets: changes in whole-cell currents and relative changes in membrane resistance induced by K_{ATP} channel modulators, respectively.
(D) Whole cell current-voltage relationships measured under diazoxide (green trace) and tolbutamide (red trace). K_{ATP} I/V curve (black trace) obtained by subtracting the curve under diazoxide by the curve under tolbutamide. The arrow indicates the reversal potential of K_{ATP} currents.
(E-H) Histograms summarizing the K_{ATP} current reversal potential (E,F) and relative K_{ATP} conductance (G,H) in identified neuronal subtypes (E,G) or between glutamatergic and GABAergic neurons (F,G). Data are expressed as mean ± s.e.m., and the individual data points are depicted. n.s. not statistically significant.

Figure 2-figure supplement 1. Diazoxide-induced current is independent of ROS production.

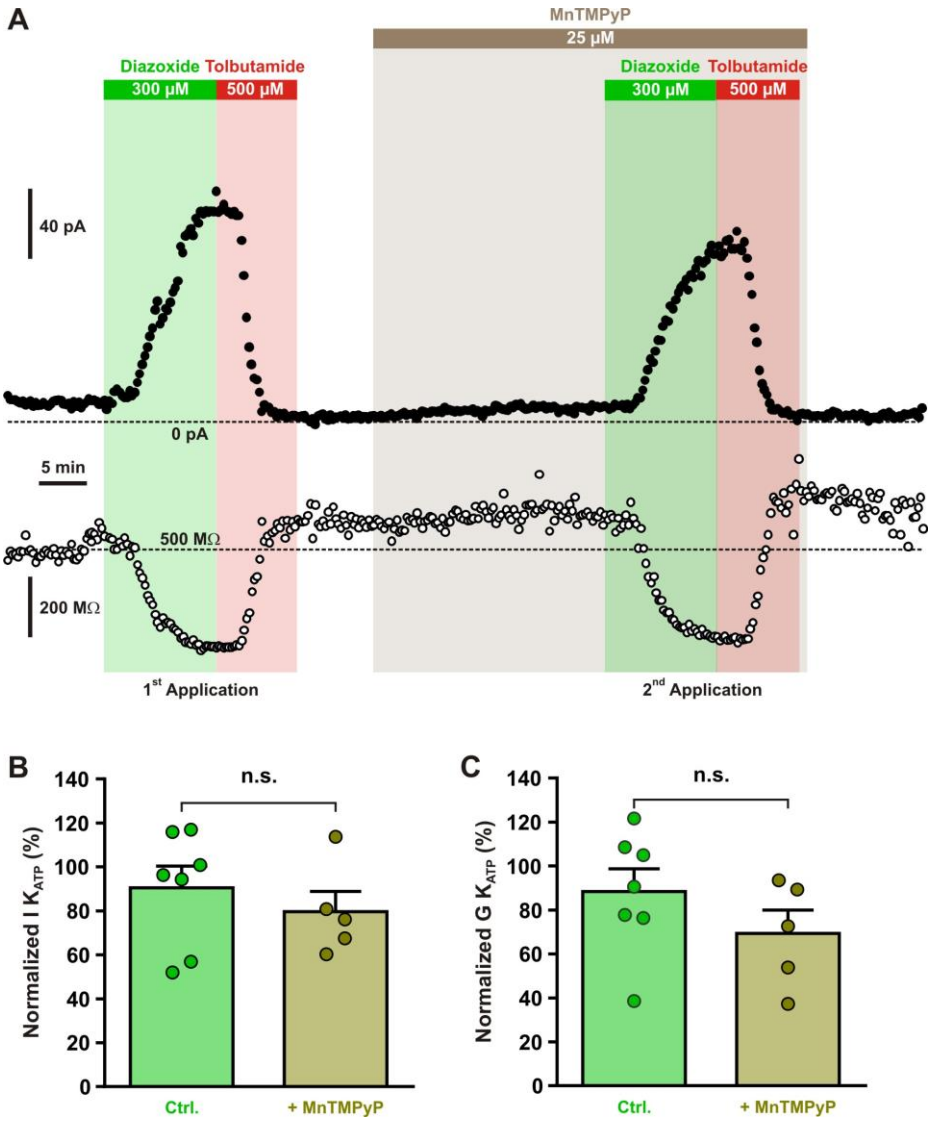

(A) Representative stationary currents at -60 mV (filled circles) and membrane resistance (open circles) changes induced by diazoxide and tolbutamide under control condition and in presence of the superoxide dismutase and catalase mimetic, MnTMPyP. The colored bars and shaded zones indicate the duration of application. (B-C) Histograms summarizing the relative K_{ATP} currents (B) and relative whole-cell K_{ATP} conductance (C) evoked by two consecutive diazoxide and tolbutamide applications in control condition (Ctrl.) and after the presence of MnTMPyP. Data are normalized by the data measured during first application, expressed as mean ± s.e.m., and the individual data points are depicted. n.s. not statistically significant.

Figure 2-figure supplement 2. Characterization of K_{ATP} channels in different cortical neurons.

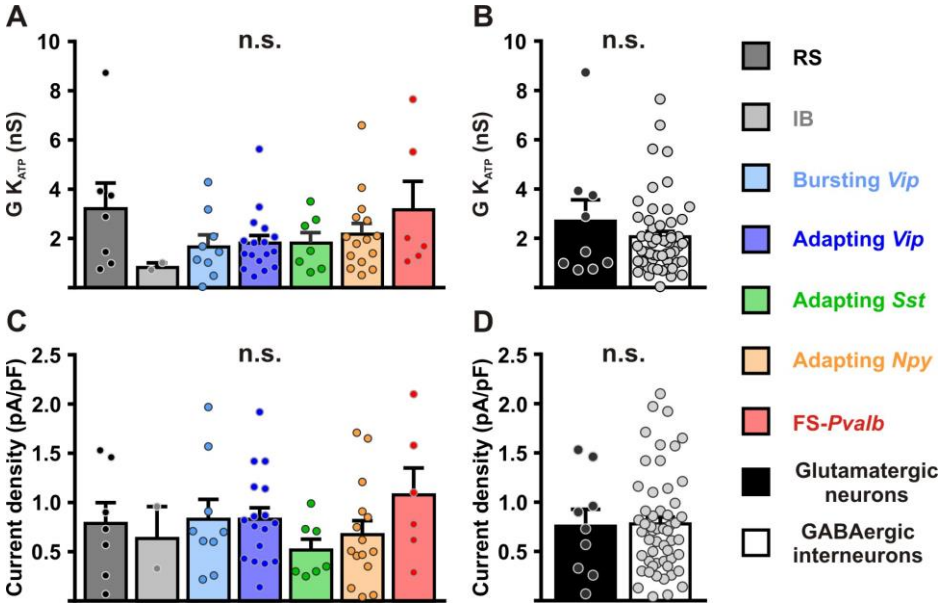

(A-D) Histograms summarizing the whole-cell K_{ATP} conductance (A, B) and K_{ATP} current density (C, D) and K_{ATP} current reversal potential in identified neuronal subtypes (A,C) or between glutamatergic and GABAergic neurons (B,D). Data are expressed as mean ± s.e.m., and the individual data points are depicted. n.s. not statistically significant.

Figure 3. KCNJ11 is the pore forming subunit of K_{ATP} channels in cortical neurons.

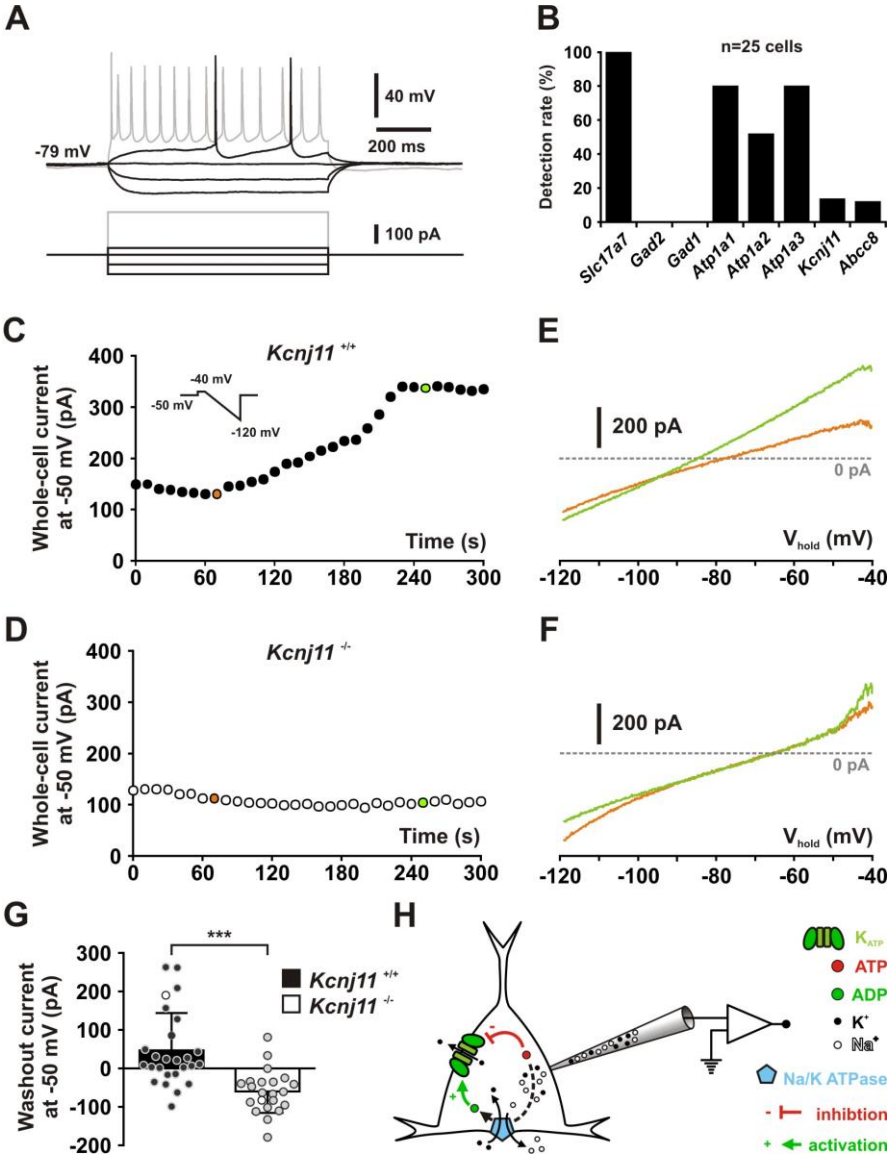

(A) Representative voltage responses of a mouse layer II/III RS pyramidal cell induced by injection of current pulses (bottom traces).

(B) Histograms summarizing the detection rate of *Slc17a7*, *Gad2* and *1*, the *Atp1a1-3* subunits of the Na/K ATPase and the *Kcnj11* and *Abcc8* K_{ATP} channel subunits in layer II/III RS pyramidal cells from *Kcnj11*$^{+/+}$ mice.

(C, D) Whole-cell stationary currents recorded at -50 mV during dialysis with ATP-free pipette solution in cortical neurons of *Kcnj11*$^{+/+}$ (C) and *Kcnj11*$^{-/-}$ (D) mice. Inset; voltage clamp protocol.

(E, F) Current-voltage relationships obtained during ATP washout at the time indicated by green and orange circles in (C, D) in cortical neurons of *Kcnj11*$^{+/+}$ (E) and *Kcnj11*$^{-/-}$ (F) mice.

(G) Histograms summarizing the whole-cell ATP washout currents in *Kcnj11*$^{+/+}$ (black) and *Kcnj11*$^{-/-}$ (white) cortical neurons. Data are expressed as mean ± s.e.m., and the individual data points are depicted. Open symbols in *Kcnj11*$^{+/+}$ and *Kcnj11*$^{-/-}$ bar plots indicate the cells illustrated in (C,D) and (E,F), respectively.

(H) Diagram depicting the principle of the ATP washout experiment.

Figure 4. Modulation of cortical neuronal excitability and activity by K_{ATP} channels.

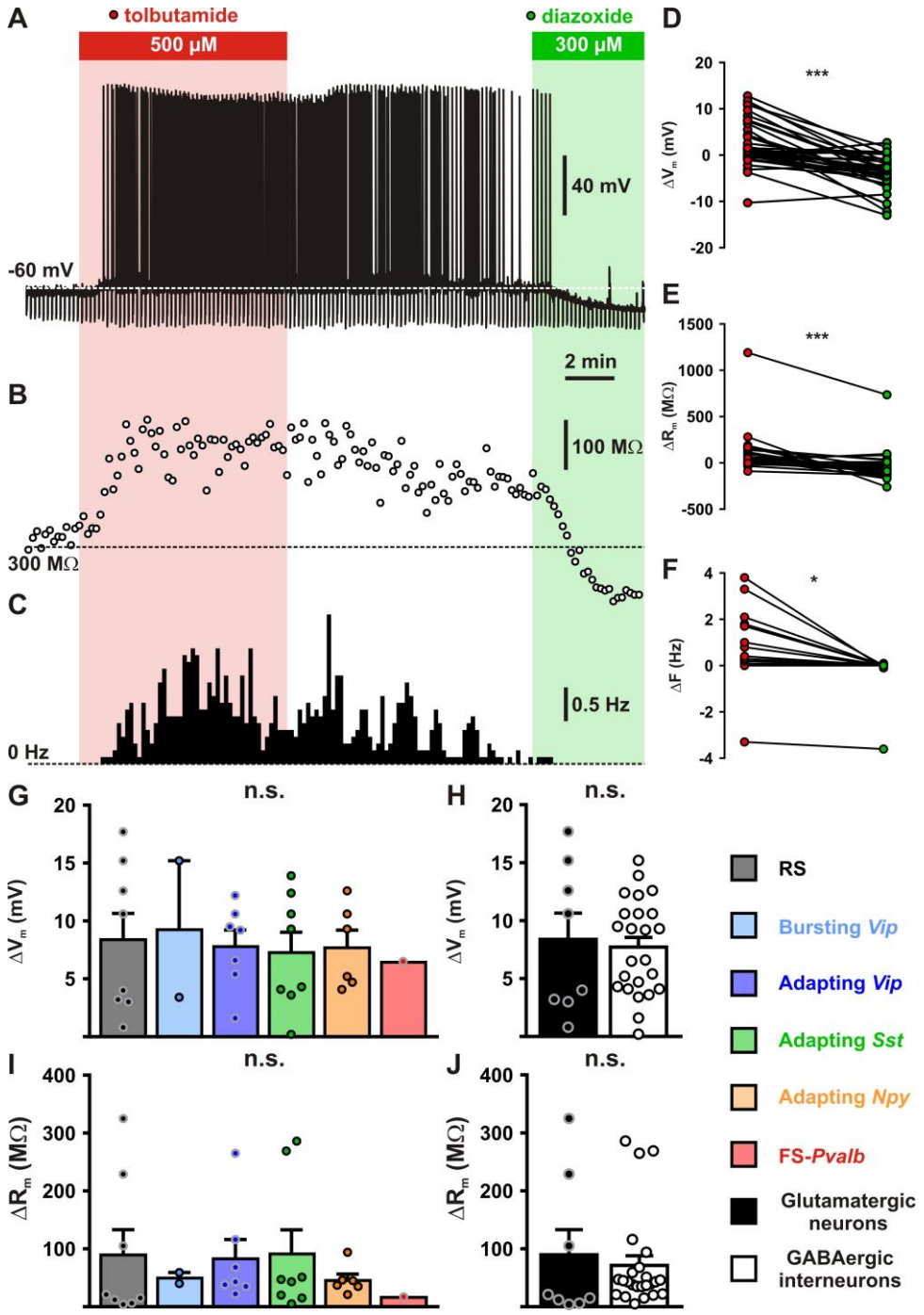

(A-C) Representative example of a RS neurons showing the changes in membrane potential (A), resistance (B, open circles) and spiking activity (C) induced by application of tolbutamide (red) and diazoxide (green). The colored bars and shaded zones indicate the application duration of K_{ATP} channel modulators.

(D-F) Relative changes in membrane potential (D), resistance (E) and firing rate (F) induced by tolbutamide and diazoxide in cortical neurons.

(G-J) Histograms summarizing the modulation of membrane potential (G, $H_{(5,32)}$= 0.15856, p=0.999, and H, $U_{(8,24)}$=96, p=1.0000) and resistance (I, $H_{(5,32)}$= 2.7566, p=0.737, and J, $U_{(8,24)}$=73, p=0.3345) by K_{ATP} channels in neuronal subtypes (G, I) and groups (H, J). Data are expressed as mean ± s.e.m., and the individual data points are depicted. n.s. not statistically significant.

Figure 4-figure supplement 1. Modulation of neuronal activity in different cortical neurons by K_{ATP} channels.

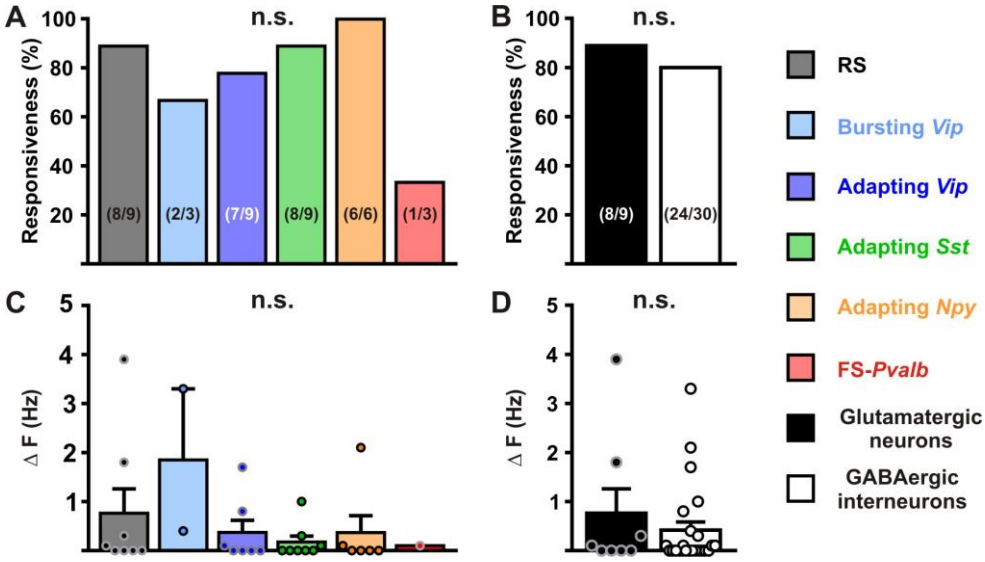

(A-D) Histograms summarizing the proportion of responsive neurons (A, $K^2_{(5)}$=7.3125, p=0.1984, and B, p=1.0000) and modulation firing rate (C, $H_{(5,32)}$= 5.0202, p=0.413, and D, $U_{(8,24)}$=87, p=0.7169) by K_{ATP} channels in neuronal subtypes (A,C) and groups (B,D). The numbers in brackets indicate the number of responsive cells and analyzed cells, respectively. Data are expressed as mean ± s.e.m., and the individual data points are depicted. n.s. not statistically significant.

Figure 5. Lactate enhances cortical neuronal activity via K_{ATP} channel modulation.

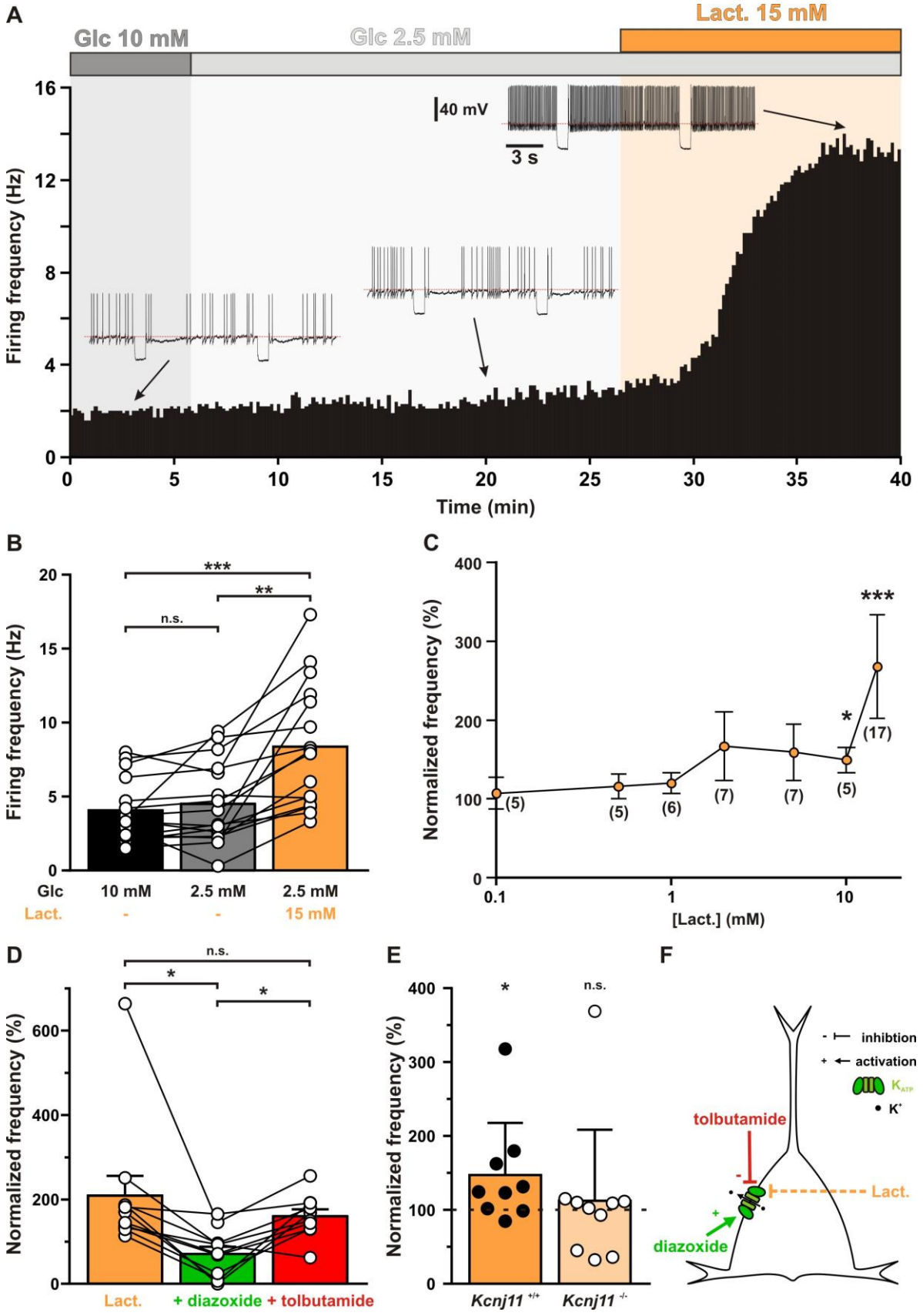

(A) Representative perforated patch recording of an adapting VIP neuron showing the modulation of firing frequency induced by changes in the extracellular concentrations of metabolites. The colored bars and shaded zones indicate the concentration in glucose (grey) and lactate (orange). Voltage responses recorded at the time indicated by arrows. The red dashed lines indicate -40 mV.

(B) Histograms summarizing the mean firing frequency during changes in extracellular concentration of glucose (black and grey) and lactate (orange). Data are expressed as mean ± s.e.m., and the individual data points are depicted. n.s. not statistically significant.

(C) Dose-dependent enhancement of firing frequency by lactate. Data are normalized by the mean firing frequency in absence of lactate and are expressed as mean ± s.e.m. Numbers in brackets indicate the number of recorded neurons at different lactate concentrations.

(D) Histograms summarizing the normalized frequency under 15 mM lactate (orange) and its modulation by addition of diazoxide (green) or tolbutamide (red). Data are expressed as mean ± s.e.m., and the individual data points are depicted. n.s. not statistically significant.

(E) Histograms summarizing the enhancement of normalized frequency by 15 mM lactate in *Kcnj11*$^{+/+}$ (orange) and *Kcnj11*$^{-/-}$ (pale orange) mouse cortical neurons. The dash line indicates the normalized mean firing frequency in absence of lactate. Data are expressed as mean ± s.e.m., and the individual data points are depicted.

(F) Diagram depicting the enhancement of neuronal activity by lactate via modulation of K_{ATP} channels.

Figure 6. Lactate enhancement of cortical neuronal activity involves lactate uptake and metabolism.

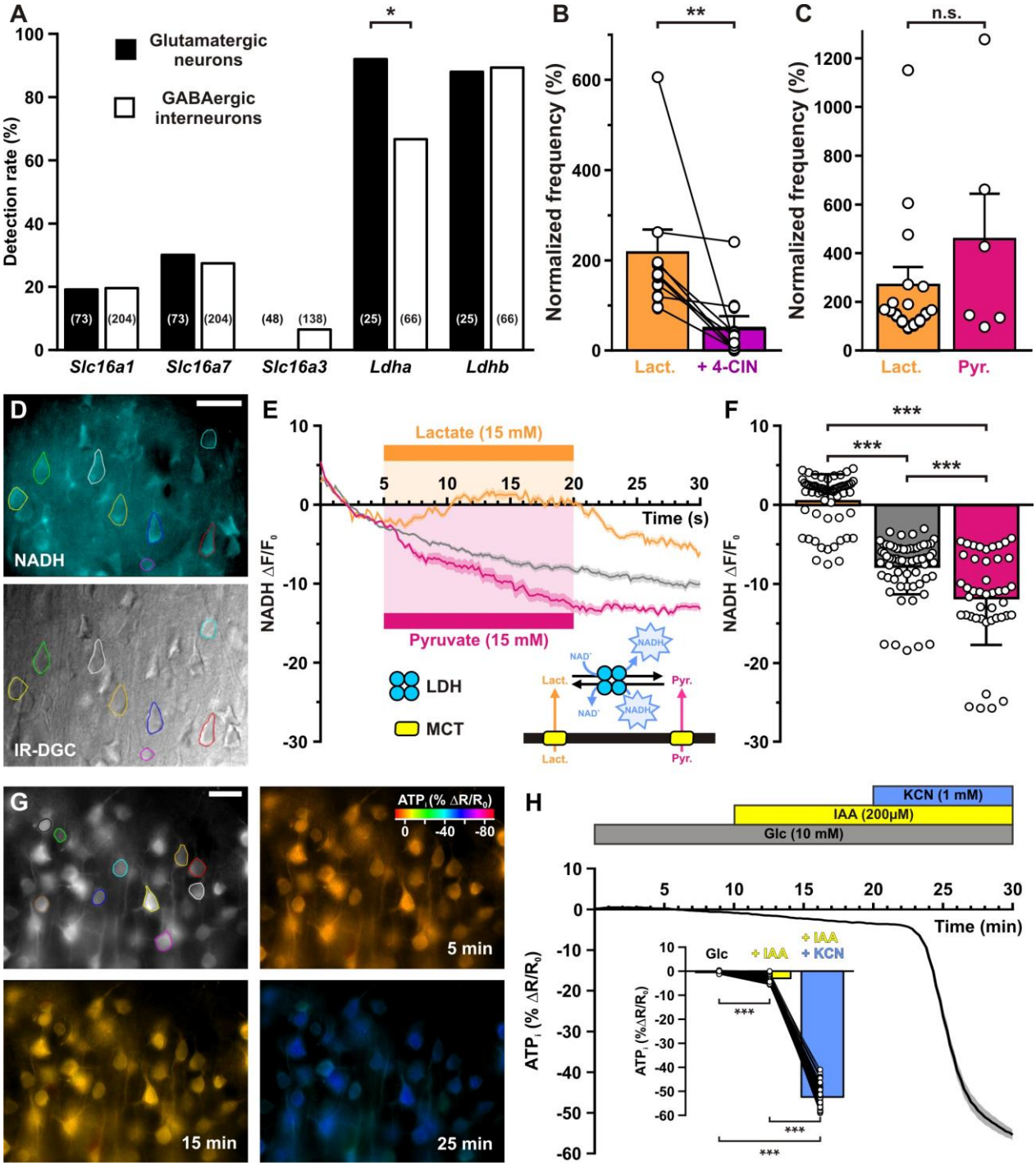

(A) Histograms summarizing the detection rate of the monocarboxylate transporters *Slc16a1*, *7* and 3 and *Ldha* and *b* lactate dehydrogenase subunits in glutamatergic neurons (black) and GABAergic interneurons (white). The numbers in brackets indicate the number of analyzed cells.

(B) Histograms summarizing the enhancement of normalized frequency by 15 mM lactate (orange) and its suppression by the MCTs inhibitor 4-CIN (purple). Data are expressed as mean ± s.e.m., and the individual data points are depicted.
(C) Histograms summarizing the enhancement of normalized frequency by 15 mM lactate (orange) and pyruvate (magenta). Data are expressed as mean ± s.e.m., and the individual data points are depicted n.s. not statistically significant.
(D) Widefield NADH autofluorescence (upper panel, scale bar: 20 µm) and corresponding field of view observed under IR-DGC (lower panel). The somatic regions of interest are delineated.
(E) Mean relative changes in NADH autofluorescence in control condition (grey) and in response to 15 mM lactate (orange) or pyruvate (magenta). The colored bars indicate the duration of applications. Data are expressed as mean ± s.e.m. Inset: diagram depicting the NADH changes induced by lactate and pyruvate uptake by MCT and their interconversion by LDH.
(F) Histograms summarizing the mean relative changes in NADH autofluorescence measured during the last 5 minutes of 15 mM lactate (orange) or pyruvate (magenta) application and corresponding time in control condition (grey). Data are expressed as mean ± s.e.m., and the individual data points are depicted.
(G) Widefield YFP fluorescence of the ATP biosensor AT1.03^{YEMK} (upper left panel, scale bar: 30 µm) and pseudocolor images showing the intracellular ATP (YFP/CFP ratio value coded by pixel hue, see scale bar in upper right panel) and the fluorescence intensity (coded by pixel intensity) at different times under 10 mM extracellular glucose (upper right panel) and after addition of IAA (lower left panel) and KCN (lower right panel).
(H) Mean relative changes in intracellular ATP (relative YFP/CFP ratio) measured under 10 mM extracellular glucose (grey) and after addition of IAA (yellow) and KCN (blue). Data are expressed as mean ± s.e.m. The colored bars indicate the time and duration of metabolic inhibitor application. Inset: Histograms summarizing the mean relative changes in intracellular ATP (relative YFP/CFP ratio) ratio under 10 mM extracellular glucose (grey) and after addition of IAA (yellow) and KCN (blue). Data are expressed as mean ± s.e.m., and the individual data points are depicted.

Figure 6-figure supplement 1. Detection rate of monocarboxylate transporters and lactate dehydrogenase subunits in different cortical neuronal types.

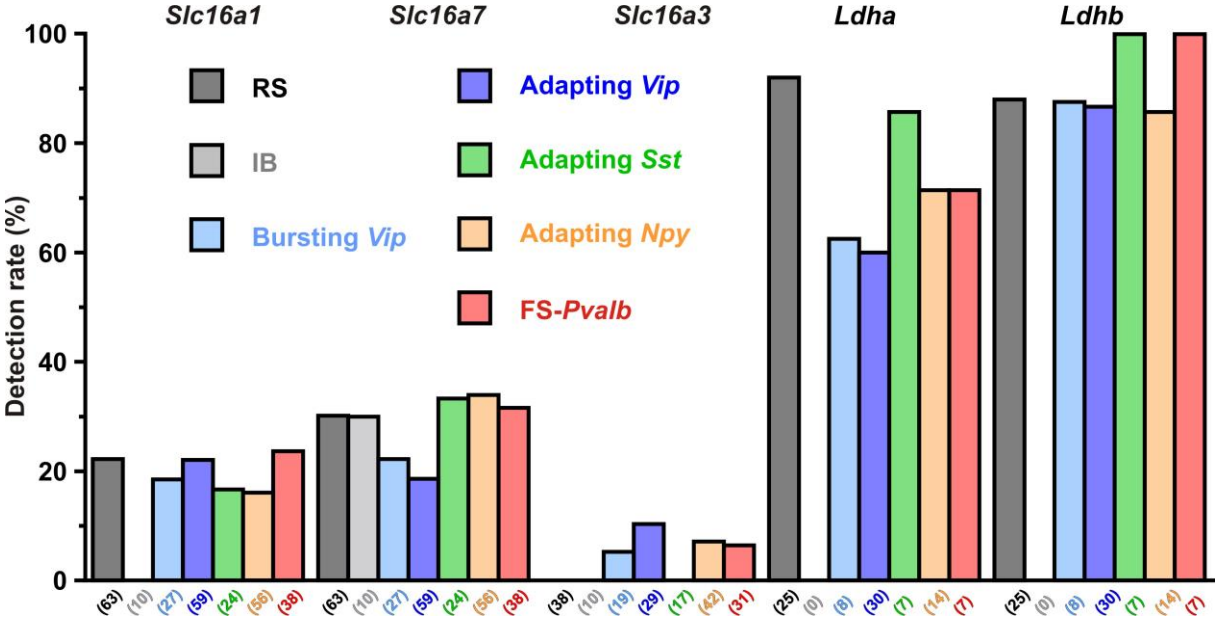

Histograms summarizing the detection rate of the monocarboxylate transporters *Slc16a1*, *7* and *3* and *Ldha* and *b* lactate dehydrogenase subunits in different neuronal subtypes. The numbers in brackets indicate the number of analyzed cells.

Figure 6-figure supplement 2. Neuronal NADH autofluorescence increase by blockade of oxidative phosphorylation.

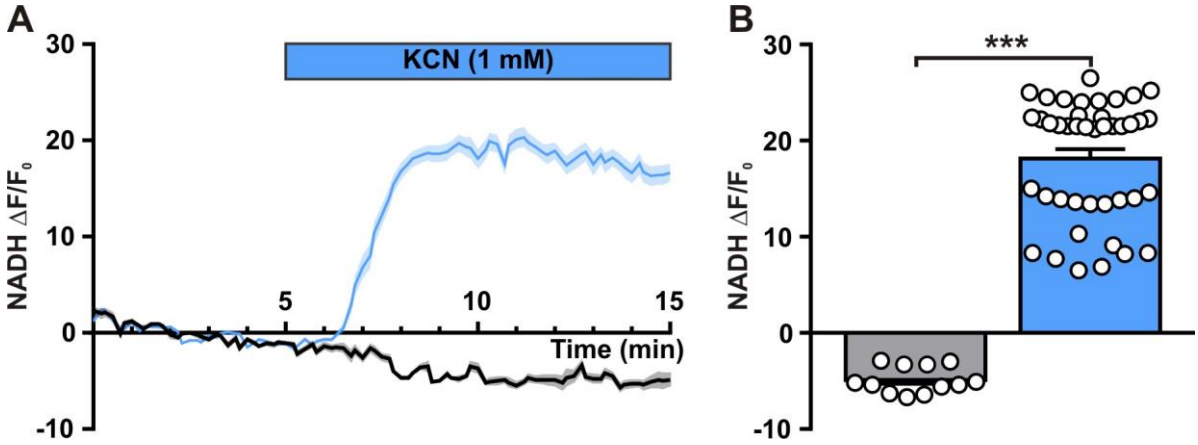

(A) Mean relative changes in NADH autofluorescence in control condition (grey) and in response to 1 mM KCN (blue). The colored bar indicates the duration of KCN applications. Data are expressed as mean ± s.e.m.

(B) Histograms summarizing the mean relative changes in NADH autofluorescence measured during the last 5 minutes of 1 mM KCN application (blue) and corresponding time in control condition (grey). Data are expressed as mean ± s.e.m., and the individual data points are depicted.

Figure 7. Diagram summarizing the mechanism of lactate-sensing in the cortical network.

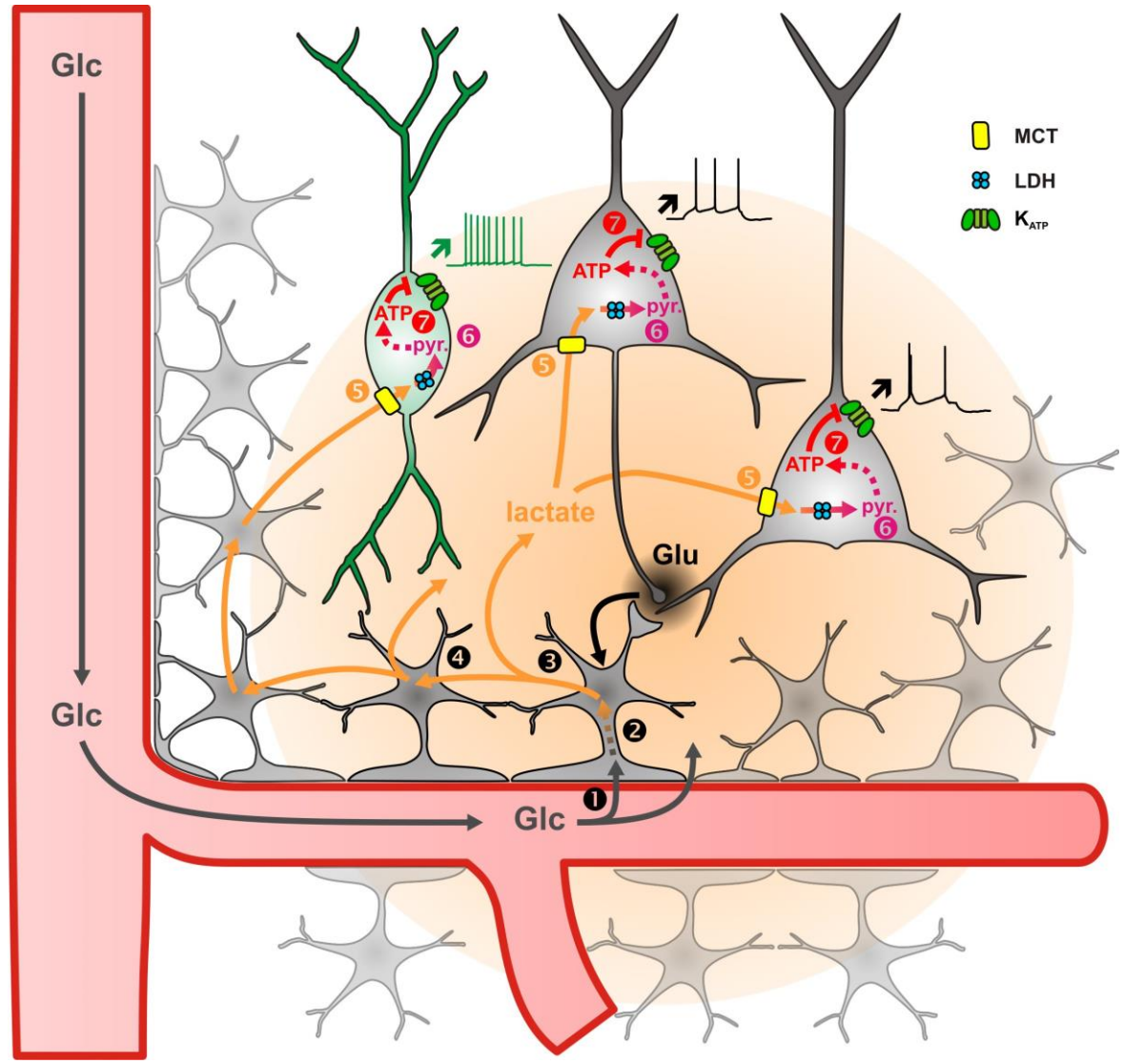

Glutamate (Glu) released during synaptic transmission stimulates ❶ blood glucose (Glc) uptake in astrocytes, ❷ aerobic glycolysis, ❸ lactate release and ❹ diffusion through the astrocytic network. Lactate is then ❺ taken up by neurons via monobarboxylate transporters (MCT) and ❻ oxidized into pyruvate by lactate dehydrogenase (LDH). The ATP produced by pyruvate oxidative metabolism ❼ closes K_{ATP} channels and increases the spiking activity of both pyramidal cells (black) and inhibitory interneurons (green). The color gradient of the circles represents the extent of glutamate (black) and lactate (orange) diffusion, respectively. Dashed arrows indicate multisteps reactions.

Supplementary file legends

Supplementary file 1. Somatic properties of different neuronal types
n, number of cells, < significantly smaller with P ≤ 0.05; << significantly smaller with P ≤ 0.01; <<< significantly smaller with P ≤ 0.001. n.s. not statistically significant.

Supplementary file 2. Detection rate of molecular markers in different neuronal types
Detection rates are given in %; n, number of cells; > significantly larger with P ≤ 0.05; >> significantly larger with P ≤ 0.01; >>> significantly larger with P ≤ 0.001. n.s. not statistically significant.

Supplementary file 3. Passive properties of different neuronal types
n, number of cells, < significantly smaller with P ≤ 0.05; << significantly smaller with P ≤ 0.01; <<< significantly smaller with P ≤ 0.001.

Supplementary file 4. Just above threshold properties of different neuronal types
n, number of cells; < significantly smaller with P ≤ 0.05; << significantly smaller with P ≤ 0.01; <<< significantly smaller with P ≤ 0.001.

Supplementary file 5. Firing properties of different neuronal types
n, number of cells; < significantly smaller with P ≤ 0.05; << significantly smaller with P ≤ 0.01; <<< significantly smaller with P ≤ 0.001.

Supplementary file 6. Action potentials properties of different neuronal types
n, number of cells; < significantly smaller with P ≤ 0.05; << significantly smaller with P ≤ 0.01; <<< significantly smaller with P ≤ 0.001.

Supplementary file 7. AH and AD properties of different neuronal types
n, number of cells; < significantly smaller with P ≤ 0.05; << significantly smaller with P ≤ 0.01; <<< significantly smaller with P ≤ 0.001.

Source data legends

Figure 1-source data 1.
Somatic, electrophysiological and molecular properties of the cortical neurons shown in Figure 1A-D.

Figure 1-source data 2.
Original file of the full raw unedited gel shown in Figure 1E.

Figure 1-source data 3.
Uncropped gel shown in Figure 1E with relevant bands labelled.

Figure 1-source data 4.
Statistcal comparisons of the detection of K_{ATP} channel subunits in different types of cortical neurons shown in Figure 1F.

Figure 1-figure supplement 1-source data 1.

Original file of the full raw unedited gel shown in Figure 1-figure supplement 1A.

Figure 1-figure supplement 1-source data 2.
Uncropped gel shown in Figure 1-figure supplement 1A with relevant lanes labelled. Yellow rectangles denote bands of the expected size.

Figure 1-figure supplement 1-source data 3.
Original file of the full raw unedited gel shown in Figure 1-figure supplement 1B.

Figure 1-figure supplement 1-source data 4.
Uncropped gel shown in Figure 1-figure supplement 1B with relevant bands labelled.

Figure 2-source data 1.
Statistical analyses of whole cell current and membrane resistance changes induced by K_{ATP} channel modulators (shown in Figure 2C insets).

Figure 2-source data 2.
Statistical comparisons of K_{ATP} current reversal potential and relative K_{ATP} conductance between neuronal subtypes and groups (shown in Figure 2E-H) and of whole-cell K_{ATP} conductance and current density (shown in Figure 2-figure supplement 2).

Figure 2-figure supplement 1-source data
Statistical analyses of the effect of MnTMPyP on normalized K_{ATP} currents and conducatnce whole-cell K_{ATP} conductance (shwon in Figure2-figure supplement 2B-C).

Figure 3-source data 2.
Molecular profile of layer II-III pyramidal neurons shown in Figure 3B.

Figure 3-source data 2.
Statistical analysis of whole-cell ATP washout currents in *Kcnj11*$^{+/+}$ and *Kcnj11*$^{-/-}$ cortical neurons (shown in Figure 3G).

Figure 4-source data 1.
Statistical analyses of membrane potential, membrane resistance and firing rate changes induced by K_{ATP} channel modulators (shwon in Figure 4D-E).

Figure 4-source data 2.
Statistical comparisons between neuronal subtypes and groups of the effect K_{ATP} channel modulators on membrane potential, membrane resistance (shwon in Figure 4 G-J) and firing rate (shwon in Figure 4- figure supplement 1 C,D) as well as of the proportion of responsive neurons (shwon in Figure 4- figure supplement 1 A,B).

Figure 5-source data 1.
Statistical analysis of the effect of glucose and lactate on firing rate (shown in Figure 5B).

Figure 5-source data 2.
Statistical analysis of dose-dependent enhancement of firing frequency by lactate (shown in Figure 5C).

Figure 5-source data 3.
Statistical analysis of the effect of diazoxide and tolbutamide on firing rate enhancement by lactate (shown in Figure 5D).

Figure 5-source data 4.
Statistical comparison of lactate enhancement of normalized frequency in $Kcnj11^{+/+}$ and $Kcnj11^{-/-}$ (shown in Figure 5E).

Figure 6-source data 1.
Statistcal comparisons of the detection rate of monocarboxylate transporters and lactate dehydrogenase subunits between neuronal groups (shown in Figure 6A) and subtypes (shown in Figure 6-figure supplement 1).

Figure 6-source data 2.
Satistical analysis of the effect of MCT inhibition by 4-CIN on lactate enhanced firing rate (shown in Figure 6B).

Figure 6-source data 3.
Statistcal comparison of the relative effect of lactate and pyruvate on firing rate enhancement (shown in Figure 6C).

Figure 6-source data 4.
Statistcal comparisons of the relative effects of lactate, pyruvate and control condition on the the mean relative changes in NADH autofluorescence (shown in Figure 6F).

Figure 6-source data 5.
Satistical analysis of the effects of IAA and KCN on the relative changes in intracellular ATP (shown in Figure 6H inset).

Figure 6-figure supplement 2-source data
Statistcal analysis of effect of KCN on the mean relative changes in NADH autofluorescence (shown in Figure 6-figure supplement 2B).

Supplementary file 1-source data.
Statistcal comparisons of somatic properties in different neuronal types.

Supplementary file 2-source data.
Statistcal comparisons of detection rate of molecular markers in different neuronal types.

Supplementary file 3-source data.
Statistcal comparisons of passive properties in different neuronal types.

Supplementary file 4-source data.
Statistcal comparisons of just above threshold properties in different neuronal types.

Supplementary file 5-source data.
Statistcal comparisons of firing properties in different neuronal types.

Supplementary file 6-source data.
Statistcal comparisons of action potentials properties in different neuronal types.

Supplementary file 7-source data.
Statistcal comparisons of AH and AD properties in different neuronal types.

References

Abi-Saab,W.M., Maggs,D.G., Jones,T., Jacob,R., Srihari,V., Thompson,J., Kerr,D., Leone,P., Krystal,J.H., Spencer,D.D., During,M.J., and Sherwin,R.S. (2002). Striking differences in glucose and lactate levels between brain extracellular fluid and plasma in conscious human subjects: effects of hyperglycemia and hypoglycemia. J. Cereb. Blood Flow Metab *22*, 271-279.

Aguilar-Bryan,L., Nichols,C.G., Wechsler,S.W., Clement,J.P., Boyd,A.E., III, Gonzalez,G., Herrera-Sosa,H., Nguy,K., Bryan,J., and Nelson,D.A. (1995). Cloning of the beta cell high-affinity sulfonylurea receptor: a regulator of insulin secretion. Science *268*, 423-426.

Ahmed,K., Tunaru,S., Tang,C., Muller,M., Gille,A., Sassmann,A., Hanson,J., and Offermanns,S. (2010). An autocrine lactate loop mediates insulin-dependent inhibition of lipolysis through GPR81. Cell Metab *11*, 311-319.

Ainscow,E.K., Mirshamsi,S., Tang,T., Ashford,M.L., and Rutter,G.A. (2002). Dynamic imaging of free cytosolic ATP concentration during fuel sensing by rat hypothalamic neurones: evidence for ATP-independent control of ATP-sensitive K(+) channels. J. Physiol *544*, 429-445.

Almeida,A., Almeida,J., Bolanos,J.P., and Moncada,S. (2001). Different responses of astrocytes and neurons to nitric oxide: the role of glycolytically generated ATP in astrocyte protection. Proc. Natl. Acad. Sci. U. S. A *98*, 15294-15299.

Ammala,C., Moorhouse,A., and Ashcroft,F.M. (1996). The sulphonylurea receptor confers diazoxide sensitivity on the inwardly rectifying K+ channel Kir6.1 expressed in human embryonic kidney cells. J. Physiol *494 (Pt 3)*, 709-714.

Ascoli,G.A., Alonso-Nanclares,L., Anderson,S.A., Barrionuevo,G., avides-Piccione,R., Burkhalter,A., Buzsaki,G., Cauli,B., DeFelipe,J., Fairen,A., Feldmeyer,D., Fishell,G., Fregnac,Y., Freund,T.F., Gardner,D., Gardner,E.P., Goldberg,J.H., Helmstaedter,M., Hestrin,S., Karube,F., Kisvarday,Z.F., Lambolez,B., Lewis,D.A., Marin,O., Markram,H., Munoz,A., Packer,A., Petersen,C.C., Rockland,K.S., Rossier,J., Rudy,B., Somogyi,P., Staiger,J.F., Tamas,G., Thomson,A.M., Toledo-Rodriguez,M., Wang,Y., West,D.C., and Yuste,R. (2008). Petilla terminology: nomenclature of features of GABAergic interneurons of the cerebral cortex. Nat. Rev. Neurosci. *9*, 557-568.

Ashford,M.L., Sturgess,N.C., Trout,N.J., Gardner,N.J., and Hales,C.N. (1988). Adenosine-5'-triphosphate-sensitive ion channels in neonatal rat cultured central neurones. Pflugers Arch. *412*, 297-304.

Attwell,D., and Laughlin,S.B. (2001). An energy budget for signaling in the grey matter of the brain. J. Cereb. Blood Flow Metab *21*, 1133-1145.

Aziz,Q., Li,Y., Anderson,N., Ojake,L., Tsisanova,E., and Tinker,A. (2017). Molecular and functional characterization of the endothelial ATP-sensitive potassium channel. J. Biol. Chem. *292*, 17587-17597.

Babenko,A.P., Aguilar-Bryan,L., and Bryan,J. (1998). A view of sur/KIR6.X, KATP channels. Annu. Rev. Physiol *60*, 667-687.

Bittar,P.G., Charnay,Y., Pellerin,L., Bouras,C., and Magistretti,P.J. (1996). Selective distribution of lactate dehydrogenase isoenzymes in neurons and astrocytes of human brain. J. Cereb. Blood Flow Metab *16*, 1079-1089.

Bondjers,C., He,L., Takemoto,M., Norlin,J., Asker,N., Hellstrom,M., Lindahl,P., and Betsholtz,C. (2006). Microarray analysis of blood microvessels from PDGF-B and PDGF-Rbeta mutant mice identifies novel markers for brain pericytes. FASEB J. *20*, 1703-1705.

Bouzier-Sore,A.K., Voisin,P., Bouchaud,V., Bezancon,E., Franconi,J.M., and Pellerin,L. (2006). Competition between glucose and lactate as oxidative energy substrates in both neurons and astrocytes: a comparative NMR study. Eur. J. Neurosci. *24*, 1687-1694.

Bouzier-Sore,A.K., Voisin,P., Canioni,P., Magistretti,P.J., and Pellerin,L. (2003). Lactate is a preferential oxidative energy substrate over glucose for neurons in culture. J. Cereb. Blood Flow Metab *23*, 1298-1306.

Bozzo,L., Puyal,J., and Chatton,J.Y. (2013). Lactate modulates the activity of primary cortical neurons through a receptor-mediated pathway. PLoS. ONE. *8*, e71721.

Broer,S., Broer,A., Schneider,H.P., Stegen,C., Halestrap,A.P., and Deitmer,J.W. (1999). Characterization of the high-affinity monocarboxylate transporter MCT2 in Xenopus laevis oocytes. Biochem. J. *341 (Pt 3)*, 529-535.

Broer,S., Schneider,H.P., Broer,A., Rahman,B., Hamprecht,B., and Deitmer,J.W. (1998). Characterization of the monocarboxylate transporter 1 expressed in Xenopus laevis oocytes by changes in cytosolic pH. Biochem. J. *333 (Pt 1)*, 167-174.

Cahoy,J.D., Emery,B., Kaushal,A., Foo,L.C., Zamanian,J.L., Christopherson,K.S., Xing,Y., Lubischer,J.L., Krieg,P.A., Krupenko,S.A., Thompson,W.J., and Barres,B.A. (2008). A transcriptome database for astrocytes, neurons, and oligodendrocytes: a new resource for understanding brain development and function. J. Neurosci. *28*, 264-278.

Cao,R., Higashikubo,B.T., Cardin,J., Knoblich,U., Ramos,R., Nelson,M.T., Moore,C.I., and Brumberg,J.C. (2009). Pinacidil induces vascular dilation and hyperemia in vivo and does not impact biophysical properties of neurons and astrocytes in vitro. Cleve. Clin. J. Med. *76 Suppl 2*, S80-S85.

Carrard,A., Elsayed,M., Margineanu,M., Boury-Jamot,B., Fragniere,L., Meylan,E.M., Petit,J.M., Fiumelli,H., Magistretti,P.J., and Martin,J.L. (2018). Peripheral administration of lactate produces antidepressant-like effects. Mol. Psychiatry *23*, 392-399.

Cauli,B., Audinat,E., Lambolez,B., Angulo,M.C., Ropert,N., Tsuzuki,K., Hestrin,S., and Rossier,J. (1997). Molecular and physiological diversity of cortical nonpyramidal cells. J. Neurosci. *17*, 3894-3906.

Cauli,B., Porter,J.T., Tsuzuki,K., Lambolez,B., Rossier,J., Quenet,B., and Audinat,E. (2000). Classification of fusiform neocortical interneurons based on unsupervised clustering. Proc. Natl. Acad. Sci. U. S. A *97*, 6144-6149.

Cauli,B., Tong,X.K., Rancillac,A., Serluca,N., Lambolez,B., Rossier,J., and Hamel,E. (2004). Cortical GABA interneurons in neurovascular coupling: relays for subcortical vasoactive pathways. J. Neurosci. *24*, 8940-8949.

Chance,B., Cohen,P., Jobsis,F., and Schoener,B. (1962). Intracellular oxidation-reduction states in vivo. Science *137*, 499-509.

Choi,H.B., Gordon,G.R., Zhou,N., Tai,C., Rungta,R.L., Martinez,J., Milner,T.A., Ryu,J.K., McLarnon,J.G., Tresguerres,M., Levin,L.R., Buck,J., and MacVicar,B.A. (2012). Metabolic Communication between Astrocytes and Neurons via Bicarbonate-Responsive Soluble Adenylyl Cyclase. Neuron *75*, 1094-1104.

Chuquet,J., Quilichini,P., Nimchinsky,E.A., and Buzsaki,G. (2010). Predominant Enhancement of Glucose Uptake in Astrocytes versus Neurons during Activation of the Somatosensory Cortex. J. Neurosci. *30*, 15298-15303.

Chutkow,W.A., Simon,M.C., Le Beau,M.M., and Burant,C.F. (1996). Cloning, tissue expression, and chromosomal localization of SUR2, the putative drug-binding subunit of cardiac, skeletal muscle, and vascular KATP channels. Diabetes *45*, 1439-1445.

Clarke,D.D., and Sokoloff,L. (1999). Circulation and Energy Metabolism of the Brain. In Basic Neurochemistry: Molecular, Cellular and Medical Aspects., G.J. Siegel, ed. (Philadelphia: Lippincott Williams & Wilkins), pp. 637-669.

Cunningham,M.O., Pervouchine,D.D., Racca,C., Kopell,N.J., Davies,C.H., Jones,R.S., Traub,R.D., and Whittington,M.A. (2006). Neuronal metabolism governs cortical network response state. Proc. Natl. Acad. Sci. U. S. A *103*, 5597-5601.

D'Agostino,D.P., Putnam,R.W., and Dean,J.B. (2007). Superoxide ({middle dot}O2-) production in CA1 neurons of rat hippocampal slices exposed to graded levels of oxygen. J. Neurophysiol.

de Castro Abrantes H., Briquet,M., Schmuziger,C., Restivo,L., Puyal,J., Rosenberg,N., Rocher,A.B., Offermanns,S., and Chatton,J.Y. (2019). The lactate receptor HCAR1 modulates neuronal network activity through the activation of Galpha and Gbeta subunits. J. Neurosci.

Devienne,G., Le Gac,B., Piquet,J., and Cauli,B. (2018). Single Cell Multiplex Reverse Transcription Polymerase Chain Reaction After Patch-clamp. J. Vis. Exp.

Devor,A., Hillman,E.M., Tian,P., Waeber,C., Teng,I.C., Ruvinskaya,L., Shalinsky,M.H., Zhu,H., Haslinger,R.H., Narayanan,S.N., Ulbert,I., Dunn,A.K., Lo,E.H., Rosen,B.R., Dale,A.M., Kleinfeld,D., and Boas,D.A. (2008). Stimulus-induced changes in blood flow and 2-deoxyglucose uptake dissociate in ipsilateral somatosensory cortex. J. Neurosci. *28*, 14347-14357.

Devor,A., Tian,P., Nishimura,N., Teng,I.C., Hillman,E.M., Narayanan,S.N., Ulbert,I., Boas,D.A., Kleinfeld,D., and Dale,A.M. (2007). Suppressed neuronal activity and

concurrent arteriolar vasoconstriction may explain negative blood oxygenation level-dependent signal. J. Neurosci. *27*, 4452-4459.

Dhar-Chowdhury,P., Harrell,M.D., Han,S.Y., Jankowska,D., Parachuru,L., Morrissey,A., Srivastava,S., Liu,W., Malester,B., Yoshida,H., and Coetzee,W.A. (2005). The glycolytic enzymes, glyceraldehyde-3-phosphate dehydrogenase, triose-phosphate isomerase, and pyruvate kinase are components of the K(ATP) channel macromolecular complex and regulate its function. J. Biol. Chem. *280*, 38464-38470.

Diaz-Garcia,C.M., Lahmann,C., Martinez-Francois,J.R., Li,B., Koveal,D., Nathwani,N., Rahman,M., Keller,J.P., Marvin,J.S., Looger,L.L., and Yellen,G. (2019). Quantitative in vivo imaging of neuronal glucose concentrations with a genetically encoded fluorescence lifetime sensor. J. Neurosci. Res.

Diaz-Garcia,C.M., Mongeon,R., Lahmann,C., Koveal,D., Zucker,H., and Yellen,G. (2017). Neuronal Stimulation Triggers Neuronal Glycolysis and Not Lactate Uptake. Cell Metab *26*, 361-374.

Dodt,H.U., and Zieglgansberger,W. (1998). Visualization of neuronal form and function in brain slices by infrared videomicroscopy. Histochem. J. *30*, 141-152.

Doyle,J.P., Dougherty,J.D., Heiman,M., Schmidt,E.F., Stevens,T.R., Ma,G., Bupp,S., Shrestha,P., Shah,R.D., Doughty,M.L., Gong,S., Greengard,P., and Heintz,N. (2008). Application of a translational profiling approach for the comparative analysis of CNS cell types. Cell *135*, 749-762.

Drose,S., Brandt,U., and Hanley,P.J. (2006). K+-independent actions of diazoxide question the role of inner membrane KATP channels in mitochondrial cytoprotective signaling. J. Biol. Chem. *281*, 23733-23739.

Dufer,M., Krippeit-Drews,P., Buntinas,L., Siemen,D., and Drews,G. (2002). Methyl pyruvate stimulates pancreatic beta-cells by a direct effect on KATP channels, and not as a mitochondrial substrate. Biochem. J. *368*, 817-825.

Dunn-Meynell,A.A., Rawson,N.E., and Levin,B.E. (1998). Distribution and phenotype of neurons containing the ATP-sensitive K+ channel in rat brain. Brain Res. *814*, 41-54.

El Hayek L., Khalifeh,M., Zibara,V., Abi,A.R., Emmanuel,N., Karnib,N., El-Ghandour,R., Nasrallah,P., Bilen,M., Ibrahim,P., Younes,J., Abou,H.E., Barmo,N., Jabre,V., Stephan,J.S., and Sleiman,S.F. (2019). Lactate Mediates the Effects of Exercise on Learning and Memory through SIRT1-Dependent Activation of Hippocampal Brain-Derived Neurotrophic Factor (BDNF). J. Neurosci. *39*, 2369-2382.

Fan,Y., Kong,H., Ye,X., Ding,J., and Hu,G. (2016). ATP-sensitive potassium channels: uncovering novel targets for treating depression. Brain Struct. Funct. *221*, 3111-3122.

Galeffi,F., Foster,K.A., Sadgrove,M.P., Beaver,C.J., and Turner,D.A. (2007). Lactate uptake contributes to the NAD(P)H biphasic response and tissue oxygen response

during synaptic stimulation in area CA1 of rat hippocampal slices. J. Neurochem. *103*, 2449-2461.

Gallopin,T., Geoffroy,H., Rossier,J., and Lambolez,B. (2006). Cortical sources of CRF, NKB, and CCK and their effects on pyramidal cells in the neocortex. Cereb. Cortex *16*, 1440-1452.

Galow,L.V., Schneider,J., Lewen,A., Ta,T.T., Papageorgiou,I.E., and Kann,O. (2014). Energy substrates that fuel fast neuronal network oscillations. Front Neurosci. *8*, 398.

German,M.S. (1993). Glucose sensing in pancreatic islet beta cells: the key role of glucokinase and the glycolytic intermediates. Proc. Natl. Acad. Sci. U. S. A *90*, 1781-1785.

Gimenez-Cassina,A., Martinez-Francois,J.R., Fisher,J.K., Szlyk,B., Polak,K., Wiwczar,J., Tanner,G.R., Lutas,A., Yellen,G., and Danial,N.N. (2012). BAD-Dependent Regulation of Fuel Metabolism and K(ATP) Channel Activity Confers Resistance to Epileptic Seizures. Neuron *74*, 719-730.

Girouard,H., Bonev,A.D., Hannah,R.M., Meredith,A., Aldrich,R.W., and Nelson,M.T. (2010). Astrocytic endfoot Ca2+ and BK channels determine both arteriolar dilation and constriction. Proc. Natl. Acad. Sci. U. S. A *107*, 3811-3816.

Gribble,F.M., Ashfield,R., Ammala,C., and Ashcroft,F.M. (1997). Properties of cloned ATP-sensitive K+ currents expressed in Xenopus oocytes. J. Physiol *498 (Pt 1)*, 87-98.

Gulyas,A.I., Buzsaki,G., Freund,T.F., and Hirase,H. (2006). Populations of hippocampal inhibitory neurons express different levels of cytochrome c. Eur. J. Neurosci. *23*, 2581-2594.

Gupta,A., Wang,Y., and Markram,H. (2000). Organizing principles for a diversity of GABAergic interneurons and synapses in the neocortex. Science *287*, 273-278.

Haj-Dahmane,S., and Andrade,R. (1997). Calcium-activated cation nonselective current contributes to the fast afterdepolarization in rat prefrontal cortex neurons. J. Neurophysiol. *78*, 1983-1989.

Halabisky,B.E., Shen,F., Huguenard,J.R., and Prince,D.A. (2006). Electrophysiological Classification of Somatostatin-positive Interneurons in Mouse Sensorimotor Cortex. J. Neurophysiol.

Hall,C.N., Klein-Flugge,M.C., Howarth,C., and Attwell,D. (2012). Oxidative phosphorylation, not glycolysis, powers presynaptic and postsynaptic mechanisms underlying brain information processing. J. Neurosci. *32*, 8940-8951.

Heron-Milhavet,L., Xue-Jun,Y., Vannucci,S.J., Wood,T.L., Willing,L.B., Stannard,B., Hernandez-Sanchez,C., Mobbs,C., Virsolvy,A., and LeRoith,D. (2004). Protection against hypoxic-ischemic injury in transgenic mice overexpressing Kir6.2 channel pore in forebrain. Mol. Cell Neurosci. *25*, 585-593.

1517 Hill,E.L., Gallopin,T., Férézou,I., Cauli,B., Rossier,J., Schweitzer,P., and Lambolez,B.
1518 (2007). Functional CB1 receptors are broadly expressed in neocortical GABAergic
1519 and glutamatergic neurons. J. Neurophysiol. *97*, 2580-2589.

1520 Houades,V., Koulakoff,A., Ezan,P., Seif,I., and Giaume,C. (2008). Gap junction-
1521 mediated astrocytic networks in the mouse barrel cortex. J. Neurosci. *28*, 5207-5217.

1522 Hu,Y., and Wilson,G.S. (1997a). A temporary local energy pool coupled to neuronal
1523 activity: fluctuations of extracellular lactate levels in rat brain monitored with rapid-
1524 response enzyme-based sensor. J. Neurochem. *69*, 1484-1490.

1525 Hu,Y., and Wilson,G.S. (1997b). Rapid changes in local extracellular rat brain
1526 glucose observed with an in vivo glucose sensor. J. Neurochem. *68*, 1745-1752.

1527 Imamura,H., Nhat,K.P., Togawa,H., Saito,K., Iino,R., Kato-Yamada,Y., Nagai,T., and
1528 Noji,H. (2009). Visualization of ATP levels inside single living cells with fluorescence
1529 resonance energy transfer-based genetically encoded indicators. Proc. Natl. Acad.
1530 Sci. U. S. A *106*, 15651-15656.

1531 Inagaki,N., Gonoi,T., Clement,J.P., Namba,N., Inazawa,J., Gonzalez,G., guilar-
1532 Bryan,L., Seino,S., and Bryan,J. (1995a). Reconstitution of IKATP: an inward rectifier
1533 subunit plus the sulfonylurea receptor. Science *270*, 1166-1170.

1534 Inagaki,N., Gonoi,T., Clement,J.P., Wang,C.Z., Aguilar-Bryan,L., Bryan,J., and
1535 Seino,S. (1996). A family of sulfonylurea receptors determines the pharmacological
1536 properties of ATP-sensitive K+ channels. Neuron *16*, 1011-1017.

1537 Inagaki,N., Tsuura,Y., Namba,N., Masuda,K., Gonoi,T., Horie,M., Seino,Y.,
1538 Mizuta,M., and Seino,S. (1995b). Cloning and functional characterization of a novel
1539 ATP-sensitive potassium channel ubiquitously expressed in rat tissues, including
1540 pancreatic islets, pituitary, skeletal muscle, and heart. J. Biol. Chem. *270*, 5691-5694.

1541 Isomoto,S., Kondo,C., Yamada,M., Matsumoto,S., Higashiguchi,O., Horio,Y.,
1542 Matsuzawa,Y., and Kurachi,Y. (1996). A novel sulfonylurea receptor forms with BIR
1543 (Kir6.2) a smooth muscle type ATP-sensitive K+ channel. J. Biol. Chem. *271*, 24321-
1544 24324.

1545 Isomoto,S., and Kurachi,Y. (1997). Function, regulation, pharmacology, and
1546 molecular structure of ATP-sensitive K+ channels in the cardiovascular system. J.
1547 Cardiovasc. Electrophysiol. *8*, 1431-1446.

1548 Ivanov,A., Mukhtarov,M., Bregestovski,P., and Zilberter,Y. (2011). Lactate Effectively
1549 Covers Energy Demands during Neuronal Network Activity in Neonatal Hippocampal
1550 Slices. Front Neuroenergetics. *3*, 2.

1551 Ivanov,A.I., Malkov,A.E., Waseem,T., Mukhtarov,M., Buldakova,S., Gubkina,O.,
1552 Zilberter,M., and Zilberter,Y. (2014). Glycolysis and oxidative phosphorylation in
1553 neurons and astrocytes during network activity in hippocampal slices. J. Cereb.
1554 Blood Flow Metab *34*, 397-407.

1555 Jimenez-Blasco,D., Busquets-Garcia,A., Hebert-Chatelain,E., Serrat,R., Vicente-
1556 Gutierrez,C., Ioannidou,C., Gomez-Sotres,P., Lopez-Fabuel,I., Resch-Beusher,M.,

Resel,E., Arnouil,D., Saraswat,D., Varilh,M., Cannich,A., Julio-Kalajzic,F., Bonilla-Del,R., I, Almeida,A., Puente,N., Achicallende,S., Lopez-Rodriguez,M.L., Jolle,C., Deglon,N., Pellerin,L., Josephine,C., Bonvento,G., Panatier,A., Lutz,B., Piazza,P.V., Guzman,M., Bellocchio,L., Bouzier-Sore,A.K., Grandes,P., Bolanos,J.P., and Marsicano,G. (2020). Glucose metabolism links astroglial mitochondria to cannabinoid effects. Nature.

Kann,O., Papageorgiou,I.E., and Draguhn,A. (2014). Highly energized inhibitory interneurons are a central element for information processing in cortical networks. J. Cereb. Blood Flow Metab *34*, 1270-1282.

Karagiannis,A., Gallopin,T., David,C., Battaglia,D., Geoffroy,H., Rossier,J., Hillman,E.M., Staiger,J.F., and Cauli,B. (2009). Classification of NPY-expressing neocortical interneurons. J. Neurosci. *29*, 3642-3659.

Karagiannis,A., Sylantyev,S., Hadjihambi,A., Hosford,P.S., Kasparov,S., and Gourine,A.V. (2015). Hemichannel-mediated release of lactate. J. Cereb. Blood Flow Metab.

Karschin,C., Ecke,C., Ashcroft,F.M., and Karschin,A. (1997). Overlapping distribution of K(ATP) channel-forming Kir6.2 subunit and the sulfonylurea receptor SUR1 in rodent brain. FEBS Lett. *401*, 59-64.

Kawaguchi,Y. (1993). Groupings of nonpyramidal and pyramidal cells with specific physiological and morphological characteristics in rat frontal cortex. J. Neurophysiol. *69*, 416-431.

Kawaguchi,Y. (1995). Physiological subgroups of nonpyramidal cells with specific morphological characteristics in layer II/III of rat frontal cortex. J. Neurosci. *15*, 2638-2655.

Kawamura,M., Jr., Ruskin,D.N., and Masino,S.A. (2010). Metabolic Autocrine Regulation of Neurons Involves Cooperation among Pannexin Hemichannels, Adenosine Receptors, and KATP Channels. J. Neurosci. *30*, 3886-3895.

Krawchuk,M.B., Ruff,C.F., Yang,X., Ross,S.E., and Vazquez,A.L. (2019). Optogenetic assessment of VIP, PV, SOM and NOS inhibitory neuron activity and cerebral blood flow regulation in mouse somato-sensory cortex 1. J. Cereb. Blood Flow Metab 271678X19870105.

Lacroix,A., Toussay,X., Anenberg,E., Lecrux,C., Ferreiros,N., Karagiannis,A., Plaisier,F., Chausson,P., Jarlier,F., Burgess,S.A., Hillman,E.M., Tegeder,I., Murphy,T.H., Hamel,E., and Cauli,B. (2015). COX-2-Derived Prostaglandin E2 Produced by Pyramidal Neurons Contributes to Neurovascular Coupling in the Rodent Cerebral Cortex. J. Neurosci. *35*, 11791-11810.

Lambolez,B., Audinat,E., Bochet,P., Crepel,F., and Rossier,J. (1992). AMPA receptor subunits expressed by single Purkinje cells. Neuron *9*, 247-258.

Laughton,J.D., Charnay,Y., Belloir,B., Pellerin,L., Magistretti,P.J., and Bouras,C. (2000). Differential messenger RNA distribution of lactate dehydrogenase LDH-1 and LDH-5 isoforms in the rat brain. Neuroscience *96*, 619-625.

Lauritzen,K.H., Morland,C., Puchades,M., Holm-Hansen,S., Hagelin,E.M., Lauritzen,F., Attramadal,H., Storm-Mathisen,J., Gjedde,A., and Bergersen,L.H. (2014). Lactate receptor sites link neurotransmission, neurovascular coupling, and brain energy metabolism. Cereb. Cortex *24*, 2784-2795.

Le Douce J., Maugard,M., Veran,J., Matos,M., Jego,P., Vigneron,P.A., Faivre,E., Toussay,X., Vandenberghe,M., Balbastre,Y., Piquet,J., Guiot,E., Tran,N.T., Taverna,M., Marinesco,S., Koyanagi,A., Furuya,S., Gaudin-Guerif,M., Goutal,S., Ghettas,A., Pruvost,A., Bemelmans,A.P., Gaillard,M.C., Cambon,K., Stimmer,L., Sazdovitch,V., Duyckaerts,C., Knott,G., Herard,A.S., Delzescaux,T., Hantraye,P., Brouillet,E., Cauli,B., Oliet,S.H.R., Panatier,A., and Bonvento,G. (2020). Impairment of Glycolysis-Derived l-Serine Production in Astrocytes Contributes to Cognitive Deficits in Alzheimer's Disease. Cell Metab *31*, 503-517.

Lee,K.P.K., Chen,J., and MacKinnon,R. (2017). Molecular structure of human KATP in complex with ATP and ADP. Elife. *6*.

Lee,Y., Morrison,B.M., Li,Y., Lengacher,S., Farah,M.H., Hoffman,P.N., Liu,Y., Tsingalia,A., Jin,L., Zhang,P.W., Pellerin,L., Magistretti,P.J., and Rothstein,J.D. (2012). Oligodendroglia metabolically support axons and contribute to neurodegeneration. Nature.

Lemak,M.S., Voloshanenko,O., Draguhn,A., and Egorov,A.V. (2014). KATP channels modulate intrinsic firing activity of immature entorhinal cortex layer III neurons. Front Cell Neurosci. *8*, 255.

Lennie,P. (2003). The cost of cortical computation. Curr. Biol. *13*, 493-497.

Lerchundi,R., Fernandez-Moncada,I., Contreras-Baeza,Y., Sotelo-Hitschfeld,T., Machler,P., Wyss,M.T., Stobart,J., Baeza-Lehnert,F., Alegria,K., Weber,B., and Barros,L.F. (2015). NH4+ triggers the release of astrocytic lactate via mitochondrial pyruvate shunting. Proc. Natl. Acad. Sci. U. S. A.

Li,N., Wu,J.X., Ding,D., Cheng,J., Gao,N., and Chen,L. (2017). Structure of a Pancreatic ATP-Sensitive Potassium Channel. Cell *168*, 101-110.

Liss,B., Bruns,R., and Roeper,J. (1999). Alternative sulfonylurea receptor expression defines metabolic sensitivity of K-ATP channels in dopaminergic midbrain neurons. EMBO J. *18*, 833-846.

Logothetis,N.K. (2008). What we can do and what we cannot do with fMRI. Nature *453*, 869-878.

Lundgaard,I., Li,B., Xie,L., Kang,H., Sanggaard,S., Haswell,J.D., Sun,W., Goldman,S., Blekot,S., Nielsen,M., Takano,T., Deane,R., and Nedergaard,M. (2015). Direct neuronal glucose uptake heralds activity-dependent increases in cerebral metabolism. Nat. Commun. *6*, 6807.

Machler,P., Wyss,M.T., Elsayed,M., Stobart,J., Gutierrez,R., von Faber-Castell,A., Kaelin,V., Zuend,M., San,M.A., Romero-Gomez,I., Baeza-Lehnert,F., Lengacher,S., Schneider,B.L., Aebischer,P., Magistretti,P.J., Barros,L.F., and Weber,B. (2016). In

Vivo Evidence for a Lactate Gradient from Astrocytes to Neurons. Cell Metab *23*, 94-102.

Magistretti,P.J., and Allaman,I. (2018). Lactate in the brain: from metabolic end-product to signalling molecule. Nat. Rev. Neurosci. *19*, 235-249.

Martin,G.M., Yoshioka,C., Rex,E.A., Fay,J.F., Xie,Q., Whorton,M.R., Chen,J.Z., and Shyng,S.L. (2017). Cryo-EM structure of the ATP-sensitive potassium channel illuminates mechanisms of assembly and gating. Elife. *6*.

Matsumoto,N., Komiyama,S., and Akaike,N. (2002). Pre- and postsynaptic ATP-sensitive potassium channels during metabolic inhibition of rat hippocampal CA1 neurons. J. Physiol *541*, 511-520.

Miki,T., Liss,B., Minami,K., Shiuchi,T., Saraya,A., Kashima,Y., Horiuchi,M., Ashcroft,F., Minokoshi,Y., Roeper,J., and Seino,S. (2001). ATP-sensitive K+ channels in the hypothalamus are essential for the maintenance of glucose homeostasis. Nat. Neurosci. *4*, 507-512.

Miki,T., Nagashima,K., Tashiro,F., Kotake,K., Yoshitomi,H., Tamamoto,A., Gonoi,T., Iwanaga,T., Miyazaki,J., and Seino,S. (1998). Defective insulin secretion and enhanced insulin action in KATP channel-deficient mice. Proc. Natl. Acad. Sci. U. S. A *95*, 10402-10406.

Molnar,G., Farago,N., Kocsis,A.K., Rozsa,M., Lovas,S., Boldog,E., Baldi,R., Csajbok,E., Gardi,J., Puskas,L.G., and Tamas,G. (2014). GABAergic neurogliaform cells represent local sources of insulin in the cerebral cortex. J. Neurosci. *34*, 1133-1137.

Moreau,C., Prost,A.L., Derand,R., and Vivaudou,M. (2005). SUR, ABC proteins targeted by KATP channel openers. J. Mol. Cell Cardiol. *38*, 951-963.

Newgard,C.B., and McGarry,J.D. (1995). Metabolic coupling factors in pancreatic beta-cell signal transduction. Annu. Rev. Biochem. *64*, 689-719.

Ogawa,M., Watabe,H., Teramoto,N., Miyake,Y., Hayashi,T., Iida,H., Murata,T., and Magata,Y. (2005). Understanding of cerebral energy metabolism by dynamic living brain slice imaging system with [18F]FDG. Neurosci. Res. *52*, 357-361.

Okuyama,Y., Yamada,M., Kondo,C., Satoh,E., Isomoto,S., Shindo,T., Horio,Y., Kitakaze,M., Hori,M., and Kurachi,Y. (1998). The effects of nucleotides and potassium channel openers on the SUR2A/Kir6.2 complex K+ channel expressed in a mammalian cell line, HEK293T cells. Pflugers Arch. *435*, 595-603.

Pellerin,L., and Magistretti,P.J. (1994). Glutamate uptake into astrocytes stimulates aerobic glycolysis: a mechanism coupling neuronal activity to glucose utilization. Proc. Natl. Acad. Sci. U. S. A. *91*, 10625-9.

Pierre,K., and Pellerin,L. (2005). Monocarboxylate transporters in the central nervous system: distribution, regulation and function. J. Neurochem. *94*, 1-14.

Piquet,J., Toussay,X., Hepp,R., Lerchundi,R., Le,D.J., Faivre,E., Guiot,E., Bonvento,G., and Cauli,B. (2018). Supragranular Pyramidal Cells Exhibit Early Metabolic Alterations in the 3xTg-AD Mouse Model of Alzheimer's Disease. Front Cell Neurosci. *12*, 216.

Prichard,J., Rothman,D., Novotny,E., Petroff,O., Kuwabara,T., Avison,M., Howseman,A., Hanstock,C., and Shulman,R. (1991). Lactate rise detected by 1H NMR in human visual cortex during physiologic stimulation. Proc. Natl. Acad. Sci. U. S. A *88*, 5829-5831.

Puljung,M.C. (2018). Cryo-electron microscopy structures and progress toward a dynamic understanding of KATP channels. J. Gen. Physiol *150*, 653-669.

Pullen,T.J., da,S., X, Kelsey,G., and Rutter,G.A. (2011). miR-29a and miR-29b contribute to pancreatic beta-cell-specific silencing of monocarboxylate transporter 1 (Mct1). Mol. Cell Biol. *31*, 3182-3194.

Quistorff,B., Secher,N.H., and Van Lieshout,J.J. (2008). Lactate fuels the human brain during exercise. FASEB J. *22*, 3443-3449.

Raichle,M.E., and Mintun,M.A. (2006). Brain work and brain imaging. Annu. Rev. Neurosci. *29*, 449-476.

Rouach,N., Koulakoff,A., Abudara,V., Willecke,K., and Giaume,C. (2008). Astroglial metabolic networks sustain hippocampal synaptic transmission. Science *322*, 1551-1555.

Ruminot,I., Gutierrez,R., Pena-Munzenmayer,G., Anazco,C., Sotelo-Hitschfeld,T., Lerchundi,R., Niemeyer,M.I., Shull,G.E., and Barros,L.F. (2011). NBCe1 Mediates the Acute Stimulation of Astrocytic Glycolysis by Extracellular K+. J. Neurosci. *31*, 14264-14271.

Sada,N., Lee,S., Katsu,T., Otsuki,T., and Inoue,T. (2015). Epilepsy treatment. Targeting LDH enzymes with a stiripentol analog to treat epilepsy. Science *347*, 1362-1367.

Sakura,H., Ammala,C., Smith,P.A., Gribble,F.M., and Ashcroft,F.M. (1995). Cloning and functional expression of the cDNA encoding a novel ATP-sensitive potassium channel subunit expressed in pancreatic beta-cells, brain, heart and skeletal muscle. FEBS Lett. *377*, 338-344.

Saunders,A., Macosko,E.Z., Wysoker,A., Goldman,M., Krienen,F.M., de,R.H., Bien,E., Baum,M., Bortolin,L., Wang,S., Goeva,A., Nemesh,J., Kamitaki,N., Brumbaugh,S., Kulp,D., and McCarroll,S.A. (2018). Molecular Diversity and Specializations among the Cells of the Adult Mouse Brain. Cell *174*, 1015-1030.

Schindelin,J., rganda-Carreras,I., Frise,E., Kaynig,V., Longair,M., Pietzsch,T., Preibisch,S., Rueden,C., Saalfeld,S., Schmid,B., Tinevez,J.Y., White,D.J., Hartenstein,V., Eliceiri,K., Tomancak,P., and Cardona,A. (2012). Fiji: an open-source platform for biological-image analysis. Nat. Methods *9*, 676-682.

Schurr,A., Miller,J.J., Payne,R.S., and Rigor,B.M. (1999). An increase in lactate output by brain tissue serves to meet the energy needs of glutamate-activated neurons. J. Neurosci. *19*, 34-39.

Schurr,A., West,C.A., and Rigor,B.M. (1988). Lactate-supported synaptic function in the rat hippocampal slice preparation. Science *240*, 1326-1328.

Sekine,N., Cirulli,V., Regazzi,R., Brown,L.J., Gine,E., Tamarit-Rodriguez,J., Girotti,M., Marie,S., MacDonald,M.J., Wollheim,C.B., and . (1994). Low lactate dehydrogenase and high mitochondrial glycerol phosphate dehydrogenase in pancreatic beta-cells. Potential role in nutrient sensing. J. Biol. Chem. *269*, 4895-4902.

Shmuel,A., Augath,M., Oeltermann,A., and Logothetis,N.K. (2006). Negative functional MRI response correlates with decreases in neuronal activity in monkey visual area V1. Nat. Neurosci. *9*, 569-577.

Shmuel,A., Yacoub,E., Pfeuffer,J., Van de Moortele,P.F., Adriany,G., Hu,X., and Ugurbil,K. (2002). Sustained negative BOLD, blood flow and oxygen consumption response and its coupling to the positive response in the human brain. Neuron *36*, 1195-1210.

Silver,I.A., and Erecinska,M. (1994). Extracellular glucose concentration in mammalian brain: continuous monitoring of changes during increased neuronal activity and upon limitation in oxygen supply in normo-, hypo-, and hyperglycemic animals. J. Neurosci. *14*, 5068-5076.

Song,Z., and Routh,V.H. (2005). Differential effects of glucose and lactate on glucosensing neurons in the ventromedial hypothalamic nucleus. Diabetes *54*, 15-22.

Sotelo-Hitschfeld,T., Niemeyer,M.I., Machler,P., Ruminot,I., Lerchundi,R., Wyss,M.T., Stobart,J., Fernandez-Moncada,I., Valdebenito,R., Garrido-Gerter,P., Contreras-Baeza,Y., Schneider,B.L., Aebischer,P., Lengacher,S., San,M.A., Le,D.J., Bonvento,G., Magistretti,P.J., Sepulveda,F.V., Weber,B., and Barros,L.F. (2015). Channel-mediated lactate release by k+-stimulated astrocytes. J. Neurosci. *35*, 4168-4178.

Stella,N., Schweitzer,P., and Piomelli,D. (1997). A second endogenous cannabinoid that modulates long-term potentiation. Nature *388*, 773-778.

Sun,H.S., Feng,Z.P., Miki,T., Seino,S., and French,R.J. (2006). Enhanced neuronal damage after ischemic insults in mice lacking Kir6.2-containing ATP-sensitive K+ channels. J. Neurophysiol. *95*, 2590-2601.

Suzuki,A., Stern,S.A., Bozdagi,O., Huntley,G.W., Walker,R.H., Magistretti,P.J., and Alberini,C.M. (2011). Astrocyte-neuron lactate transport is required for long-term memory formation. Cell *144*, 810-823.

Tanaka,T., Nagashima,K., Inagaki,N., Kioka,H., Takashima,S., Fukuoka,H., Noji,H., Kakizuka,A., and Imamura,H. (2014). Glucose-stimulated single pancreatic islets sustain increased cytosolic ATP levels during initial Ca2+ influx and subsequent Ca2+ oscillations. J. Biol. Chem. *289*, 2205-2216.

1756 Tanner,G.R., Lutas,A., Martinez-Francois,J.R., and Yellen,G. (2011). Single K ATP
1757 channel opening in response to action potential firing in mouse dentate granule
1758 neurons. J. Neurosci. *31*, 8689-8696.

1759 Tantama,M., Martinez-Francois,J.R., Mongeon,R., and Yellen,G. (2013). Imaging
1760 energy status in live cells with a fluorescent biosensor of the intracellular ATP-to-ADP
1761 ratio. Nat. Commun. *4*, 2550.

1762 Tarasov,A.I., Girard,C.A., and Ashcroft,F.M. (2006). ATP sensitivity of the ATP-
1763 sensitive K+ channel in intact and permeabilized pancreatic beta-cells. Diabetes *55*,
1764 2446-2454.

1765 Tasic,B., Menon,V., Nguyen,T.N., Kim,T.K., Jarsky,T., Yao,Z., Levi,B., Gray,L.T.,
1766 Sorensen,S.A., Dolbeare,T., Bertagnolli,D., Goldy,J., Shapovalova,N., Parry,S.,
1767 Lee,C., Smith,K., Bernard,A., Madisen,L., Sunkin,S.M., Hawrylycz,M., Koch,C., and
1768 Zeng,H. (2016). Adult mouse cortical cell taxonomy revealed by single cell
1769 transcriptomics. Nat. Neurosci.

1770 Thevenaz,P., Ruttimann,U.E., and Unser,M. (1998). A pyramid approach to subpixel
1771 registration based on intensity. IEEE Trans. Image Process *7*, 27-41.

1772 Thomzig,A., Laube,G., Pruss,H., and Veh,R.W. (2005). Pore-forming subunits of K-
1773 ATP channels, Kir6.1 and Kir6.2, display prominent differences in regional and
1774 cellular distribution in the rat brain. J. Comp Neurol. *484*, 313-330.

1775 Thomzig,A., Wenzel,M., Karschin,C., Eaton,M.J., Skatchkov,S.N., Karschin,A., and
1776 Veh,R.W. (2001). Kir6.1 is the principal pore-forming subunit of astrocyte but not
1777 neuronal plasma membrane K-ATP channels. Mol. Cell Neurosci. *18*, 671-690.

1778 Tsuzuki,K., Lambolez,B., Rossier,J., and Ozawa,S. (2001). Absolute quantification of
1779 AMPA receptor subunit mRNAs in single hippocampal neurons. J. Neurochem. *77*,
1780 1650-1659.

1781 Uhlirova,H., Kilic,K., Tian,P., Thunemann,M., Desjardins,M., Saisan,P.A.,
1782 Sakadzic,S., Ness,T.V., Mateo,C., Cheng,Q., Weldy,K.L., Razoux,F.,
1783 Vanderberghe,M., Cremonesi,J.A., Ferri,C.G., Nizar,K., Sridhar,V.B., Steed,T.C.,
1784 Abashin,M., Fainman,Y., Masliah,E., Djurovic,S., Andreassen,O., Silva,G.A.,
1785 Boas,D.A., Kleinfeld,D., Buxton,R.B., Einevoll,G.T., Dale,A.M., and Devor,A. (2016).
1786 Cell type specificity of neurovascular coupling in cerebral cortex. Elife. *5*.

1787 Vanlandewijck,M., He,L., Mae,M.A., Andrae,J., Ando,K., Del,G.F., Nahar,K.,
1788 Lebouvier,T., Lavina,B., Gouveia,L., Sun,Y., Raschperger,E., Rasanen,M., Zarb,Y.,
1789 Mochizuki,N., Keller,A., Lendahl,U., and Betsholtz,C. (2018). A molecular atlas of cell
1790 types and zonation in the brain vasculature. Nature *554*, 475-480.

1791 Varin,C., Rancillac,A., Geoffroy,H., Arthaud,S., Fort,P., and Gallopin,T. (2015).
1792 Glucose Induces Slow-Wave Sleep by Exciting the Sleep-Promoting Neurons in the
1793 Ventrolateral Preoptic Nucleus: A New Link between Sleep and Metabolism. J.
1794 Neurosci. *35*, 9900-9911.

1795 Vezzoli,E., Cali,C., De,R.M., Ponzoni,L., Sogne,E., Gagnon,N., Francolini,M.,
1796 Braida,D., Sala,M., Muller,D., Falqui,A., and Magistretti,P.J. (2020). Ultrastructural

Evidence for a Role of Astrocytes and Glycogen-Derived Lactate in Learning-Dependent Synaptic Stabilization. Cereb. Cortex *30*, 2114-2127.

Voutsinos-Porche,B., Bonvento,G., Tanaka,K., Steiner,P., Welker,E., Chatton,J.Y., Magistretti,P.J., and Pellerin,L. (2003). Glial glutamate transporters mediate a functional metabolic crosstalk between neurons and astrocytes in the mouse developing cortex. Neuron *37*, 275-286.

Ward,J.H. (1963). Hierarchical grouping to optimize an objective function. Journal of the American Statistical Association *58*, 236-244.

Wilson,J.E. (2003). Isozymes of mammalian hexokinase: structure, subcellular localization and metabolic function. J. Exp. Biol. *206*, 2049-2057.

Wyss,M.T., Jolivet,R., Buck,A., Magistretti,P.J., and Weber,B. (2011). In vivo evidence for lactate as a neuronal energy source. J. Neurosci. *31*, 7477-7485.

Xi,Q., Cheranov,S.Y., and Jaggar,J.H. (2005). Mitochondria-derived reactive oxygen species dilate cerebral arteries by activating Ca2+ sparks. Circ. Res. *97*, 354-362.

Yamada,M., Isomoto,S., Matsumoto,S., Kondo,C., Shindo,T., Horio,Y., and Kurachi,Y. (1997). Sulphonylurea receptor 2B and Kir6.1 form a sulphonylurea-sensitive but ATP-insensitive K+ channel. J. Physiol *499 (Pt 3)*, 715-720.

Yang,X.J., Kow,L.M., Funabashi,T., and Mobbs,C.V. (1999). Hypothalamic glucose sensor: similarities to and differences from pancreatic beta-cell mechanisms. Diabetes *48*, 1763-1772.

Zawar,C., and Neumcke,B. (2000). Differential activation of ATP-sensitive potassium channels during energy depletion in CA1 pyramidal cells and interneurones of rat hippocampus. Pflugers Arch. *439*, 256-262.

Zawar,C., Plant,T.D., Schirra,C., Konnerth,A., and Neumcke,B. (1999). Cell-type specific expression of ATP-sensitive potassium channels in the rat hippocampus. J. Physiol *514 (Pt 2)*, 327-341.

Zeisel,A., Manchado,A.B., Codeluppi,S., Lonnerberg,P., La,M.G., Jureus,A., Marques,S., Munguba,H., He,L., Betsholtz,C., Rolny,C., Castelo-Branco,G., Hjerling-Leffler,J., and Linnarsson,S. (2015). Cell types in the mouse cortex and hippocampus revealed by single-cell RNA-seq. Science.

Zilberter,Y., Zilberter,T., and Bregestovski,P. (2010). Neuronal activity in vitro and the in vivo reality: the role of energy homeostasis. Trends Pharmacol. Sci. *31*, 394-401.

Key Resources Table				
Reagent type (species) or resource	**Designation**	**Source or reference**	**Identifiers**	**Additional information**
strain, strain background (*Rattus norvegicus,* Wistar, male)	Wistar	Janvier Labs	jHan:WI	
strain, strain background (*Mus musculus* , C57BL/6RJ, male and female)	Wild type, *Kcnj11* $^{+/+}$	Janvier Labs	C57BL/6 RJ	
strain, strain background (*Mus musculus* , B6.129P2, male and female)	B6.129P2-*Kcnj11*^{tm1Sse}, Kcnj11 $^{-/-}$	PMID: 9724715 (Miki et al., 1998)	RRID: MGI:5433 111	
cell line (*Mesocricetus auratus*)	BHK-21 clone 13 (baby hamster kidneys fibroblasts)	ATCC	CCL-10, RRID: CVCL_19 15	
recombinant DNA reagent	pcDNA-ATeam1.03YEM K (plasmid)	PMID: 19720993 (Imamura et al., 2009)		
recombinant DNA reagent	pSinRep5 (plasmid)	Invitrogen	K750-01	
recombinant DNA reagent	pDH(26S) (helper plasmid)	Invitrogen	K750-01	
sequence-based reagent	rat *Slc17a7* external sense	PMID: 16339088 (Gallopin et al., 2006)	PCR primers	GGCTCCTTTT TCTGGGGGT AC
sequence-based reagent	rat *Slc17a7* external antisense	PMID: 16339088 (Gallopin et al., 2006)	PCR primers	CCAGCCGAC TCCGTTCTAA G

sequence-based reagent	rat *Slc17a7* internal sense	PMID: 16339088 (Gallopin et al., 2006)	PCR primers	TGGGGGTAC ATTGTCACTC AGA
sequence-based reagent	rat *Slc17a7* internal antisense	PMID: 16339088 (Gallopin et al., 2006)	PCR primers	ATGGCAAGC AGGGTATGT GAC
sequence-based reagent	rat/mouse *Gad2* external sense	PMID: 19295167 (Karagiannis et al., 2009)	PCR primers	CCAAAAGTTC ACGGGCGG
sequence-based reagent	rat/mouse *Gad2* external antisense	PMID: 19295167 (Karagiannis et al., 2009)	PCR primers	TCCTCCAGAT TTTGCGGTTG
sequence-based reagent	rat *Gad2* internal sense	PMID: 19295167 (Karagiannis et al., 2009)	PCR primers	TGAGAAGCC AGCAGAGAG CG
sequence-based reagent	rat *Gad2* internal antisense	PMID: 19295167 (Karagiannis et al., 2009)	PCR primers	TGGGGTAAT GGAAATCAAT CACTT
sequence-based reagent	rat *Gad1* external sense	PMID: 19295167 (Karagiannis et al., 2009)	PCR primers	ATGATACTTG GTGTGGCGT AGC
sequence-based reagent	rat *Gad1* external antisense	PMID: 19295167 (Karagiannis et al., 2009)	PCR primers	GTTTGCTCCT CCCCGTTCTT AG
sequence-based reagent	rat *Gad1* internal sense	PMID: 19295167 (Karagiannis et al., 2009)	PCR primers	CAATAGCCTG GAAGAGAAG AGTCG
sequence-based reagent	rat *Gad1* internal antisense	PMID: 19295167 (Karagiannis et al., 2009)	PCR primers	GTTTGCTCCT CCCCGTTCTT AG

sequence-based reagent	rat *Nos1* external sense	PMID: 19295167 (Karagiannis et al., 2009)	PCR primers	CCTGGGGCT CAAATGGTAT G
sequence-based reagent	rat *Nos1* external antisense	PMID: 19295167 (Karagiannis et al., 2009)	PCR primers	CACAATCCAC ACCCAGTCG G
sequence-based reagent	rat *Nos1* internal sense	PMID: 19295167 (Karagiannis et al., 2009)	PCR primers	CCTCCCCGC TGTGTCCAA
sequence-based reagent	rat *Nos1* internal antisense	PMID: 19295167 (Karagiannis et al., 2009)	PCR primers	GAGTGGTGG TCAACGATG GTCA
sequence-based reagent	rat *Calb1* external sense	PMID: 19295167 (Karagiannis et al., 2009)	PCR primers	GAAAGAAGG CTGGATTGGA G
sequence-based reagent	rat *Calb1* external antisense	PMID: 19295167 (Karagiannis et al., 2009)	PCR primers	CCCACACATT TTGATTCCCT G
sequence-based reagent	rat *Calb1* internal sense	PMID: 19295167 (Karagiannis et al., 2009)	PCR primers	ATGGGCAGA GAGATGATG GG
sequence-based reagent	rat *Calb1* internal antisense	PMID: 19295167 (Karagiannis et al., 2009)	PCR primers	TATCATCCAC GGTCTTGTTT GC
sequence-based reagent	rat *Pvalb* external sense	PMID: 19295167 (Karagiannis et al., 2009)	PCR primers	GCCTGAAGA AAAAGAGTG CGG
sequence-based reagent	rat *Pvalb* external antisense	PMID: 19295167 (Karagiannis et al., 2009)	PCR primers	GTCCCCGTC CTTGTCTCCA G

sequence-based reagent	rat *Pvalb* internal sense	PMID: 19295167 (Karagiannis et al., 2009)	PCR primers	GCGGATGAT GTGAAGAAG GTG
sequence-based reagent	rat *Pvalb* internal antisense	PMID: 19295167 (Karagiannis et al., 2009)	PCR primers	CAGCCATCA GCGTCTTTGT T
sequence-based reagent	rat *Calb2* external sense	PMID: 19295167 (Karagiannis et al., 2009)	PCR primers	TTGATGCTGA CGGAAATGG GTA
sequence-based reagent	rat *Calb2* external antisense	PMID: 19295167 (Karagiannis et al., 2009)	PCR primers	CAAGCCTCC ATAAACTCAG CG
sequence-based reagent	rat *Calb2* internal sense	PMID: 19295167 (Karagiannis et al., 2009)	PCR primers	GCTGGAGAA GGCAAGGAA AGG
sequence-based reagent	rat *Calb2* internal antisense	PMID: 19295167 (Karagiannis et al., 2009)	PCR primers	ATTCTCTTCG GTTGGCAGG A
sequence-based reagent	rat *Npy* external sense	PMID: 19295167 (Karagiannis et al., 2009)	PCR primers	CGAATGGGG CTGTGTGGA
sequence-based reagent	rat *Npy* external antisense	PMID: 19295167 (Karagiannis et al., 2009)	PCR primers	AGTTTCATTT CCCATCACCA CAT
sequence-based reagent	rat *Npy* internal sense	PMID: 19295167 (Karagiannis et al., 2009)	PCR primers	CCCTCGCTCT ATCCCTGCTC
sequence-based reagent	rat *Npy* internal antisense	PMID: 19295167 (Karagiannis et al., 2009)	PCR primers	GTTCTGGGG GCATTTTCTG TG

sequence-based reagent	rat *Vip* external sense	PMID: 19295167 (Karagiannis et al., 2009)	PCR primers	TTATGATGTG TCCAGAAATG CGAG
sequence-based reagent	rat *Vip* external antisense	PMID: 19295167 (Karagiannis et al., 2009)	PCR primers	TTTTATTTGG TTTTGCTATG GAAG
sequence-based reagent	rat *Vip* internal sense	PMID: 19295167 (Karagiannis et al., 2009)	PCR primers	TGGCAAACG AATCAGCAGT AGC
sequence-based reagent	rat *Vip* internal antisense	PMID: 19295167 (Karagiannis et al., 2009)	PCR primers	GAATCTCCCT CACTGCTCCT CT
sequence-based reagent	rat *Sst* external sense	PMID: 19295167 (Karagiannis et al., 2009)	PCR primers	ATGCTGTCCT GCCGTCTCC A
sequence-based reagent	rat *Sst* external antisense	PMID: 17068095 (Férézou et al., 2007)	PCR primers	GCCTCATCTC GTCCTGCTCA
sequence-based reagent	rat *Sst* internal sense	PMID: 19295167 (Karagiannis et al., 2009)	PCR primers	GCATCGTCCT GGCTTTGGG
sequence-based reagent	rat *Sst* internal antisense	PMID: 19295167 (Karagiannis et al., 2009)	PCR primers	AGGCTCCAG GGCATCGTTC T
sequence-based reagent	rat *Cck* external sense	PMID: 19295167 (Karagiannis et al., 2009)	PCR primers	TGTCTGTGCG TGGTGATGG C
sequence-based reagent	rat *Cck* external antisense	PMID: 19295167 (Karagiannis et al., 2009)	PCR primers	GCATAGCAA CATTAGGTCT GGGAG

sequence-based reagent	rat *Cck* internal sense	PMID: 19295167 (Karagiannis et al., 2009)	PCR primers	ATACATCCAG CAGGTCCGC AA
sequence-based reagent	rat *Cck* internal antisense	PMID: 19295167 (Karagiannis et al., 2009)	PCR primers	GGTCGTGTG CGTGGTTGTT T
sequence-based reagent	rat *Kcnj8* external sense	This paper	PCR primers	CTGGCTCACA AGAACATCC G
sequence-based reagent	rat *Kcnj8* external antisense	This paper	PCR primers	AGCGTCTCTG CCCTTCTGTG
sequence-based reagent	rat *Kcnj8* internal sense	PMID: 26156991 (Varin et al., 2015)	PCR primers	GCTGGCTGC TCTTCGCTAT C
sequence-based reagent	rat *Kcnj8* internal antisense	This paper	PCR primers	TTCTCCCTCC AAACCCAATG
sequence-based reagent	rat *Kcnj11* external sense	This paper	PCR primers	CCCCACACG CTGCTCATTT T
sequence-based reagent	rat *Kcnj11* external antisense	This paper	PCR primers	AGGAGCCAG GTCGTAGAG CG
sequence-based reagent	rat *Kcnj11* internal sense	This paper	PCR primers	GCGTCACAA GCATCCACTC C
sequence-based reagent	rat *Kcnj11* internal antisense	This paper	PCR primers	CCACCCACA CCGTTCTCCA T

sequence-based reagent	rat *Abcc8* external sense	This paper	PCR primers	GGTGAAGAA GCCTCCGAT GA
sequence-based reagent	rat *Abcc8* external antisense	This paper	PCR primers	GGTGAAGAA GCCTCCGAT GA
sequence-based reagent	rat *Abcc8* internal sense	This paper	PCR primers	GGTTCGGTC CACTGTCAAG G
sequence-based reagent	rat *Abcc8* internal antisense	This paper	PCR primers	GTCAGCGTCT CCATCCGTG C
sequence-based reagent	rat *Abcc9* external sense	This paper	PCR primers	CGCTGCCTTT TGAGTCCTGT
sequence-based reagent	rat *Abcc9* external antisense	This paper	PCR primers	GATGGCAAG GAGGAGAGA CG
sequence-based reagent	rat *Abcc9* internal sense	This paper	PCR primers	TGGACAACTA CGAGCAGGC G
sequence-based reagent	rat *Abcc9* internal antisense	This paper	PCR primers	CACAACCCA CCTGACCCA CA
sequence-based reagent	rat *Sst* intron external sense	PMID: 17267760 (Hill et al., 2007)	PCR primers	GGAAATGGC TGGGACTCG TC
sequence-based reagent	rat *Sst* intron external antisense	PMID: 17267760 (Hill et al., 2007)	PCR primers	AAACCATGGA TGATAGGAA GTCGT

sequence-based reagent	rat *Sst* intron internal sense	This paper	PCR primers	GTCCCCTTTG CGAATTCCCT
sequence-based reagent	rat *Sst* intron internal antisense	This paper	PCR primers	TTCGAGCAG CTCCATTTTC C
sequence-based reagent	rat SUR2A/B sense	This paper	PCR primers	ACTTCAGCGT TGGACAGAG ACA
sequence-based reagent	rat SUR2A/B antisense	This paper	PCR primers	GGTCAGCAG TCAGAATGGT GTG
sequence-based reagent	mouse *Slc17a7* external sense	PMID: 23565079 (Cabezas et al., 2013)	PCR primers	GGCTCCTTTT TCTGGGGCT AC
sequence-based reagent	mouse *Slc17a7* external antisense	PMID: 23565079 (Cabezas et al., 2013)	PCR primers	CCAGCCGAC TCCGTTCTAA G
sequence-based reagent	mouse *Slc17a7* internal sense	PMID: 23565079 (Cabezas et al., 2013)	PCR primers	ATTCGCAGCC AACAGGGTC T
sequence-based reagent	mouse *Slc17a7* internal antisense	PMID: 23565079 (Cabezas et al., 2013)	PCR primers	TGGCAAGCA GGGTATGTG AC
sequence-based reagent	mouse *Gad2* external sense	PMID: 22754499 (Perrenoud et al., 2012)	PCR primers	CCAAAAGTTC ACGGGCGG
sequence-based reagent	mouse *Gad2* external antisense	PMID: 22754499 (Perrenoud et al., 2012)	PCR primers	TCCTCCAGAT TTTGCGGTTG

sequence-based reagent	mouse *Gad2* internal sense	PMID: 22754499 (Perrenoud et al., 2012)	PCR primers	CACCTGCGACCAAAAACCCT
sequence-based reagent	mouse *Gad2* internal antisense	PMID: 22754499 (Perrenoud et al., 2012)	PCR primers	GATTTTGCGGTTGGTCTGCC
sequence-based reagent	mouse *Gad1* external sense	PMID: 12196560 (Férézou et al., 2002)	PCR primers	TACGGGGTTCGCACAGGTC
sequence-based reagent	mouse *Gad1* external antisense	PMID: 23565079 (Cabezas et al., 2013)	PCR primers	CCCAGGCAGCATCCACAT
sequence-based reagent	mouse *Gad1* internal sense	PMID: 23565079 (Cabezas et al., 2013)	PCR primers	CCCAGAAGTGAAGACAAAAGGC
sequence-based reagent	mouse *Gad1* internal antisense	PMID: 23565079 (Cabezas et al., 2013)	PCR primers	AATGCTCCGTAAACAGTCGTGC
sequence-based reagent	mouse *Atp1a1* external sense	PMID: 29985318 (Devienne et al., 2018)	PCR primers	CAGGGCAGTGTTTCAGGCTAA
sequence-based reagent	mouse *Atp1a1* external antisense	PMID: 29985318 (Devienne et al., 2018)	PCR primers	CCGTGGAGAAGGATGGAGC
sequence-based reagent	mouse *Atp1a1* internal sense	PMID: 29985318 (Devienne et al., 2018)	PCR primers	TAAGCGGGCAGTAGCGGG
sequence-based reagent	mouse *Atp1a1* internal antisense	PMID: 29985318 (Devienne et al., 2018)	PCR primers	AGGTGTTTGGGCTCAGATGC

sequence-based reagent	mouse *Atp1a2* external sense	PMID: 29985318 (Devienne et al., 2018)	PCR primers	AGTGAGGAA GATGAGGGA CAGG
sequence-based reagent	mouse *Atp1a2* external antisense	PMID: 29985318 (Devienne et al., 2018)	PCR primers	ACAGAAGCC CAGCACTCGT T
sequence-based reagent	mouse *Atp1a2* internal sense	PMID: 29985318 (Devienne et al., 2018)	PCR primers	AAATCCCCTT CAACTCCACC A
sequence-based reagent	mouse *Atp1a2* internal antisense	PMID: 29985318 (Devienne et al., 2018)	PCR primers	GTTCCCCAAG TCCTCCCAGC
sequence-based reagent	mouse *Atp1a3* external sense	PMID: 29985318 (Devienne et al., 2018)	PCR primers	CGGAAATACA ATACTGACTG CGTG
sequence-based reagent	mouse *Atp1a3* external antisense	PMID: 29985318 (Devienne et al., 2018)	PCR primers	GTCATCCTCC GTCCCTGCC
sequence-based reagent	mouse *Atp1a3* internal sense	PMID: 29985318 (Devienne et al., 2018)	PCR primers	TGACACACA GTAAAGCCC AGGA
sequence-based reagent	mouse *Atp1a3* internal antisense	PMID: 29985318 (Devienne et al., 2018)	PCR primers	CCACAGCAG GATAGAGAA GCCA
sequence-based reagent	mouse *Kcnj11* external sense	PMID: 29985318 (Devienne et al., 2018)	PCR primers	CGGAGAGGG CACCAATGT
sequence-based reagent	mouse *Kcnj11* external antisense	PMID: 29985318 (Devienne et al., 2018)	PCR primers	CACCCACGC CATTCTCCA

sequence-based reagent	mouse *Kcnj11* internal sense	PMID: 29985318 (Devienne et al., 2018)	PCR primers	CATCCACTCC TTTTCATCTG CC
sequence-based reagent	mouse *Kcnj11* internal antisense	PMID: 29985318 (Devienne et al., 2018)	PCR primers	TCGGGGCTG GTGGTCTTG
sequence-based reagent	mouse *Abcc8* external sense	PMID: 29985318 (Devienne et al., 2018)	PCR primers	CAGTGTGCC CCCCGAGAG
sequence-based reagent	mouse *Abcc8* external antisense	PMID: 29985318 (Devienne et al., 2018)	PCR primers	GGTCTTCTCC CTCGCTGTCT G
sequence-based reagent	mouse *Abcc8* internal sense	PMID: 29985318 (Devienne et al., 2018)	PCR primers	ATCATCGGA GGCTTCTTCA CC
sequence-based reagent	mouse *Abcc8* internal antisense	PMID: 29985318 (Devienne et al., 2018)	PCR primers	GGTCTTCTCC CTCGCTGTCT G
sequence-based reagent	mouse *Sst* intron external sense	PMID: 12930808 (Thoby-Brisson et al., 2003)	PCR primers	CTGTCCCCCT TACGAATCCC
sequence-based reagent	mouse *Sst* intron external antisense	PMID: 12930808 (Thoby-Brisson et al., 2003)	PCR primers	CCAGCACCA GGGATAGAG CC
sequence-based reagent	mouse *Sst i*ntron internal sense:	PMID: 20427660 (Cea-del Rio et al., 2010)	PCR primers	CTTACGAATC CCCCAGCCTT
sequence-based reagent	mouse *Sst* intron internal antisense	PMID: 20427660 (Cea-del Rio et al., 2010)	PCR primers	TTGAAAGCCA GGGAGGAAC T

sequence-based reagent	rat *Slc16a1* external sense	This paper	PCR primers	GTCAGCCTTC CTCCTTTCCA
sequence-based reagent	rat *Slc16a1* external antisense	This paper	PCR primers	TCCGCTTTCT GTTCTTTGGC
sequence-based reagent	rat *Slc16a1* internal sense	This paper	PCR primers	TTGTTGCGAA TGGAGTGTG C
sequence-based reagent	rat *Slc16a1* internal antisense	This paper	PCR primers	CACGCCACA AGCCCAGTAT G
sequence-based reagent	rat *Slc16a7* external sense	This paper	PCR primers	GCGAAGTCT AAAAGTAAGG TTGGC
sequence-based reagent	rat *Slc16a7* external antisense	This paper	PCR primers	ATTTACCAGC CAGGGGAGG G
sequence-based reagent	rat *Slc16a7* internal sense	This paper	PCR primers	CCGTATGCTA AGGACAAAG GAGT
sequence-based reagent	rat *Slc16a7* internal antisense	This paper	PCR primers	GGGAAGAAC TGGGCAACA CT
sequence-based reagent	rat *Slc16a3* external sense	This paper	PCR primers	CATTGGTCTC GTGCTGCTGT
sequence-based reagent	rat *Slc16a3* external antisense	This paper	PCR primers	CCCCGTTTTT CTCAGGCTCT

sequence-based reagent	rat *Slc16a3* internal sense	This paper	PCR primers	TGTGGCTGTGCTCATCGGAC
sequence-based reagent	rat *Slc16a3* internal antisense	This paper	PCR primers	CCTCTTCCTCTTCCCGATGC
sequence-based reagent	rat *Ldha* external sense	This paper	PCR primers	GAAGAACAGGTCCCCCAGAA
sequence-based reagent	rat *Ldha* external antisense	This paper	PCR primers	GGGTTTGAGACGATGAGCAGT
sequence-based reagent	rat *Ldha* internal sense	This paper	PCR primers	CAGTTGTTGGGGTTGGTGCT
sequence-based reagent	rat *Ldha* internal antisense	This paper	PCR primers	TCTCTCCCTCTTGCTGACGG
sequence-based reagent	rat *Ldhb* external sense	This paper	PCR primers	ACTGCCGTCCCGAACAACAA
sequence-based reagent	rat *Ldhb* external antisense	This paper	PCR primers	ACTCTCCCCCTCCTGCTGG
sequence-based reagent	rat *Ldhb* internal sense	This paper	PCR primers	TCTGGGGAAGTCTCTGGCTGA
sequence-based reagent	rat *Ldhb* internal antisense	This paper	PCR primers	TTGGCTGTCACGGAGTAATCTTT

commercial assay or kit	MEGAscript™ SP6 Transcription Kit	Ambion	AM1330	
chemical compound, drug	Pinacidil monohydrate	Sigma-Aldrich	P154	
chemical compound, drug	Diazoxide	Sigma-Aldrich	D9035	
chemical compound, drug	Tolbutamide	Sigma-Aldrich	T0891	
chemical compound, drug	Mn(III)tetrakis(1-methyl-4-pyridyl)porphyrin	Millipore	475872	
chemical compound, drug	Gramicidin from Bacillus aneurinolyticus (Bacillus brevis)	Sigma-Aldrich	G5002	
chemical compound, drug	Sodium L-lactate	Sigma-Aldrich	L7022	
chemical compound, drug	α-Cyano-4-hydroxycinnamic Acid	Sigma-Aldrich	C2020	
chemical compound, drug	Sodium pyruvate	Sigma-Aldrich	P2256	
chemical compound, drug	Sodium iodoacetate	Sigma-Aldrich	I2512	

chemical compound, drug	Potassium cyanide	Sigma-Aldrich	60178	
chemical compound, drug	Dithiothreitol	VWR	443852A	
chemical compound, drug	Primer "random"	Roche	11034731001	
chemical compound, drug	dNTPs	GE Healthcare Life Sciences	28-4065-52	
chemical compound, drug	Mineral Oil	Sigma-Aldrich	M5904	
chemical compound, drug	RNasin Ribonuclease Inhibitors	Promega	N2511	
chemical compound, drug	SuperScript II Reverse Transcriptase	Invitrogen	18064014	
chemical compound, drug	Taq DNA Polymerase	Qiagen	201205	
chemical compound, drug	Penicillin-Streptomycin	Sigma-Aldrich	P4333-100ML	
software, algorithm	Pclamp v 10.2	Molecular Devices	RRID: SCR_011323	

software, algorithm	Matlab v 2018b	MathWorks	RRID: SCR_001622	
software, algorithm	Statistica v 6.1	Statsoft	RRID: SCR_014213	
software, algorithm	GraphPad Prism v 7	GraphPad	RRID: SCR_002798	
software, algorithm	ImagingWorkbench v 6.0.25	INDEC Systems		
software, algorithm	FIJI	PMID: 22743772 (Schindelin et al., 2012)	RRID: SCR_002285	
software, algorithm	Image-Pro Analyzer v 7	MediaCybernetics		
other	Vibratome	Leica	VT1000S RRID: SCR_016495	
other	Upright microscope	Olympus	BX51WI	
other	Dual port module	Olympus	WI-DPMC	
other	60x Objective	Olympus	LUMPlan Fl /IR 60x/0.90 W	

other	40x Objetive	Olympus	LUMPlan Fl /IR 40x/0.80 W	
other	CCD camera	Roper Scientific	CoolSnap HQ2	
other	Axopatch 200B	Molecular Devices	RRID: SCR_018866	
other	Digidata 1440A	Molecular Devices	RRID: SCR_021038	
other	S900 stimulator	Dagan corporation		
other	pE-2	CoolLED		
other	Dichroic mirror	Semrock	FF395/495/610-Di01-25x36	
other	Emission filter	Semrock	FF01-425/527/685-25	
other	780 nm Collimated LED	Thorlabs	M780L3-C1	
other	Dodt Gradient Contrast	Luigs and Neumann	200-100 200 0155	

other	Beam splitter	Semrock	725 DCSPXR	
other	Analogic CCD camera	Sony	XC ST-70 CE	
other	Millicell	Millipore	PICM0R G50	
other	Excitation filter	Semrock	FF02-438/24-25	
other	Dichroic mirror	Semrock	FF458-Di02-25x36	
other	Emission filter	Semrock	FF01-483/32-25	
other	Emission filter	Semrock	FF01-542/27-25	
other	Filter wheel	Sutter Instruments	Lambda 10B	

Cabezas,C., Irinopoulou,T., Cauli,B., and Poncer,J.C. (2013). Molecular and functional characterization of GAD67-expressing, newborn granule cells in mouse dentate gyrus. Front Neural Circuits. *7*, 60.

Cea-del Rio,C.A., Lawrence,J.J., Tricoire,L., Erdelyi,F., Szabo,G., and McBain,C.J. (2010). M3 muscarinic acetylcholine receptor expression confers differential cholinergic modulation to neurochemically distinct hippocampal basket cell subtypes. J. Neurosci. *30*, 6011-6024.

Devienne,G., Le Gac,B., Piquet,J., and Cauli,B. (2018). Single Cell Multiplex Reverse Transcription Polymerase Chain Reaction After Patch-clamp. J. Vis. Exp.

Férézou,I., Cauli,B., Hill,E.L., Rossier,J., Hamel,E., and Lambolez,B. (2002). 5-HT3 receptors mediate serotonergic fast synaptic excitation of neocortical vasoactive intestinal peptide/cholecystokinin interneurons. J. Neurosci. *22*, 7389-7397.

Férézou,I., Hill,E.L., Cauli,B., Gibelin,N., Kaneko,T., Rossier,J., and Lambolez,B. (2007). Extensive overlap of mu-opioid and nicotinic sensitivity in cortical interneurons. Cereb. Cortex *17*, 1948-1957.

Gallopin,T., Geoffroy,H., Rossier,J., and Lambolez,B. (2006). Cortical sources of CRF, NKB, and CCK and their effects on pyramidal cells in the neocortex. Cereb. Cortex *16*, 1440-1452.

Hill,E.L., Gallopin,T., Férézou,I., Cauli,B., Rossier,J., Schweitzer,P., and Lambolez,B. (2007). Functional CB1 receptors are broadly expressed in neocortical GABAergic and glutamatergic neurons. J. Neurophysiol. *97*, 2580-2589.

Imamura,H., Nhat,K.P., Togawa,H., Saito,K., Iino,R., Kato-Yamada,Y., Nagai,T., and Noji,H. (2009). Visualization of ATP levels inside single living cells with fluorescence resonance energy transfer-based genetically encoded indicators. Proc. Natl. Acad. Sci. U. S. A *106*, 15651-15656.

Karagiannis,A., Gallopin,T., David,C., Battaglia,D., Geoffroy,H., Rossier,J., Hillman,E.M., Staiger,J.F., and Cauli,B. (2009). Classification of NPY-expressing neocortical interneurons. J. Neurosci. *29*, 3642-3659.

Miki,T., Nagashima,K., Tashiro,F., Kotake,K., Yoshitomi,H., Tamamoto,A., Gonoi,T., Iwanaga,T., Miyazaki,J., and Seino,S. (1998). Defective insulin secretion and enhanced insulin action in KATP channel-deficient mice. Proc. Natl. Acad. Sci. U. S. A *95*, 10402-10406.

Perrenoud,Q., Geoffroy,H., Gauthier,B., Rancillac,A., Alfonsi,F., Kessaris,N., Rossier,J., Vitalis,T., and Gallopin,T. (2012). Characterization of Type I and Type II nNOS-Expressing Interneurons in the Barrel Cortex of Mouse. Front Neural Circuits. *6*, 36.

Thoby-Brisson,M., Cauli,B., Champagnat,J., Fortin,G., and Katz,D.M. (2003). Expression of functional tyrosine kinase B receptors by rhythmically active respiratory neurons in the pre-Botzinger complex of neonatal mice. J. Neurosci. *23*, 7685-7689.

Varin,C., Rancillac,A., Geoffroy,H., Arthaud,S., Fort,P., and Gallopin,T. (2015). Glucose Induces Slow-Wave Sleep by Exciting the Sleep-Promoting Neurons in the Ventrolateral Preoptic Nucleus: A New Link between Sleep and Metabolism. J. Neurosci. *35*, 9900-9911.